2024-08-15

Wind-carved Wonders: An Aerial Study of Yardangs in the Puna, Argentina Using Drone and Satellite Imagery

Derek Gordon Ashliman
Brigham Young University

Wind-carved Wonders: An Aerial Study of Yardangs in the Puna, Argentina Using Drone and Satellite Imagery

Derek Gordon Ashliman

A thesis submitted to the faculty of
Brigham Young University
in partial fulfillment of the requirements for the degree of

Master of Science

Jani Radebaugh, Chair
Landon Burgener
Samuel Hudson

Department of Geological Sciences
Brigham Young University

ABSTRACT

Wind-carved Wonders: An Aerial Study of Yardangs in the Puna, Argentina Using Drone and Satellite Imagery

Derek Gordon Ashliman
Department of Geological Sciences, BYU
Master of Science

Yardangs, elongated landforms sculpted by wind erosion, are prominent features in the Campo de Piedra Pomez (CPP) region of the Puna-Altiplano Plateau, Argentina. This study explores their formation and evolution through the examination of a 6 km by 0.5 km area captured in 2019 and a 5 km by 0.5 km area in 2024. High-resolution drone imagery and satellite data were employed to classify and quantify yardangs, gravel, and underlying bedrock across a vast study area. The research reveals a variation in yardang distribution and morphology from northwest (windward) to southeast (leeward), noting a significant decrease in yardang and bedrock area, coupled with an increase in gravel coverage. This linear pattern suggests a progressive formation process, highlighting varying degrees of yardang maturity influenced by wind erosion and sediment transport.

Digital Elevation Models (DEMs) indicated that elevated regions within the CPP have a higher concentration of yardangs, suggesting localized factors such as geological composition and wind exposure contribute to yardang development. Additionally, gravel analysis showed a distinct difference in size, shape, and composition along the windward-to-leeward transect: larger, more angular gravel with little quartz upwind, and smaller, well-rounded gravel with higher quartz content downwind. These findings highlight the role of prevailing northwest winds in shaping the yardangs and transporting sediment across the region.

A key aspect of this research is the proposal of a staged progression model for yardang formation, where windward yardangs are less mature and downwind yardangs exhibit more advanced erosional features. This model provides a nuanced understanding of yardang evolution and highlights the dynamic nature of aeolian processes. Furthermore, the study draws parallels with similar landforms on Mars, Venus, and Titan, suggesting that the mechanisms of yardang formation on Earth can inform our understanding of aeolian processes on other planetary bodies.

Overall, this study enhances the understanding of yardang formation and evolution, contributing valuable insights into the interaction between geological structures and atmospheric forces. The findings underscore the importance of high-resolution imagery and photogrammetry in geomorphological research and offer a foundation for future studies to explore the detailed mechanisms behind yardang formation on Earth and other planets.

Keywords: yardangs, drone, Campo de Piera Pomez, classification, gravel

ACKNOWLEDGEMENTS

This thesis represents not just my efforts, but the collective guidance and support of many who have journeyed with me throughout this academic pursuit. I am profoundly grateful to each person who contributed to my studies and supported my work.

First and foremost, I would like to extend my deepest gratitude to Brigham Young University and the Department of Geological Sciences for providing the resources, environment, and Christ centered community necessary for my research, academic, and personal growth. The facilities and scholarly atmosphere at BYU have been fundamental in shaping the direction and execution of this research.

I am particularly grateful to my research advisor, Jani Radebaugh, whose insights and expertise have been invaluable throughout this process. Her mentorship was not just academic; it was a beacon of inspiration and motivation that pushed me to rigorously explore and expand my understanding of geomorphological processes. Her guidance through the complexities of my research was pivotal in the successful completion of this thesis. I am also grateful for NASA Jet Propulsion Laboratory that provided funds to aid with our trip to Argentina and my trips to present at conferences.

Additionally, I would like to thank the other members of my committee: Landon Burgener and Sam Hudson. Their help, feedback and constructive critiques have significantly enhanced both the quality of my research and my own personal development as a scholar. Their dedication to my project and their willingness to share their profound knowledge have been greatly appreciated.

My heartfelt thanks also go to all the professors and classmates who have enriched my journey. The discussions, study sessions, and everyday interactions have not only aided my studies but have also helped me grow at a personal level. The camaraderie and support of my fellow classmates have been a source of comfort and encouragement throughout this challenging and rewarding journey.

Last but certainly not least, I must express my deepest appreciation to my parents, Jana and Gordon Ashliman. Their unwavering support and belief in my abilities have been the cornerstone of my achievements. Their sacrifices have not gone unnoticed, and their love and guidance continue to light my path. Thank you for being my constant source of encouragement and for believing in me even when the challenges seemed insurmountable.

To all who have been a part of this journey—thank you. Your collective contributions have not only made this thesis possible but have also made it a meaningful adventure in my academic and personal life.

TABLE OF CONTENTS

LIST OF FIGURES

1 Introduction

Yardangs, erosional landforms created by aeolian processes of deflation and abrasion (Ward and Greeley, 1984; Goudie, 2007), are unique geomorphological features found in various arid environments on Earth and other planetary bodies including Mars, Titan, and Venus. Despite extensive studies, considerable gaps persist in understanding the precise formation mechanisms of yardangs and the specific environmental factors that influence their development. This study aims to address these gaps by looking at the sizes, shapes and distribution of yardangs and gravels on the Puna-Altiplano Plateau of Argentina.

The Puna, a region within the Central Andes Mountains spanning across Bolivia and Argentina, is characterized by hyper arid conditions, strong winds, and high elevations. As a result of these conditions and the erodible substrate, the primary landforms on this regional plateau are yardangs, which are etched into young volcanic ash flow tuff deposits from several different volcanoes (de Silva et al., 2010). The youngest yardangs in the Puna are found within the Campo de Piedra Pomez (CPP), a 130 km² area of rhyolitic ignimbrite from the 55-75 ka eruption of the Cerro Blanco or Robledo Caldera. These yardangs (FIGURE 1) are characterized by their parallel

Figure 1; A 1.73m tall geologist standing on top of a yardang in the Campo de Piedra Pomez, Argentina.

elongated axes, regular width, and spacing (Goudie, 2007). Yardangs exhibit a remarkable size range: micro-yardangs measure mere centimeters in both height and

length, meso-yardangs span several meters, and mega-yardangs rise tens of meters high and extend over several kilometers (Goudie, 2007). The meso-yardangs of the CPP are free of vegetation and evidence of liquid water, enabling the observation of wind-surface dynamics and geological evolution. These features are among the most promising on Earth for revealing the progressive stages from their emergence to maturity, which are still not understood (de Silva et al. 2010; Barchyn and Hugenholtz, 2015; Pelletier et al. 2018).

Employing high-resolution drone and satellite imagery, this study aims to meticulously chart and analyze the morphologies and spatial distributions of yardangs within the CPP. A classification analysis was conducted to analyze raster images to delineate distinct geomorphological features, such as yardangs, gravel, and bedrock. A change detection analysis was performed using orthomosaics from the 2019 and 2024 research trips in the same location to observe temporal transformations in the yardang field. The results discuss patterns and correlations that help reveal evolutionary aspects of the yardang field.

Existing research has examined yardang formation and morphology across diverse global and planetary locations, revealing both universal principles and unique characteristics influenced by local geological and climatic conditions. Building upon previous findings, this study delves deeper into the Puna Plateau's yardang fields, aiming to elucidate the finer details of their morphologies and spatial arrangements, thereby addressing the existing knowledge gaps. The following sections detail the methodologies employed, present the findings, and discuss their implications in the broader context of geomorphological and planetary science research.

2 Yardang Background

Yardangs, globally distributed, develop in diverse rock types under unimodal wind conditions, exemplifying the universal nature of aeolian erosion processes. (Goudie, 2007).

Research from the Ocotillo Wells region in California demonstrates how yardang aspect ratios are influenced by both the geological orientation of bedrock (dip and strike) and the prevailing wind direction. Larger yardangs exhibit gentler side slopes,

with heights increasing as the square root of their width (Pelletier et al., 2018). Similarly, the teardrop shape of yardangs, approaching an ideal 1:4 width-to-length ratio, results from sequential erosion processes observed in wind-tunnel simulations where abrasion and deflation are key mechanisms (Greeley, 1993).

In the Qaidam Basin, China, yardangs are classified into four types based on their width-to-length ratios: short-axis, whale-back, hogsback, and long-ridge. This classification, driven by sedimentary rock structures and relative wind shear forces, provides a nuanced understanding of yardang geometries (Hu et al., 2017). In the Qaidam Basin, yardangs located in syncline areas exhibit higher length-to-width ratios than those in anticline areas, underscoring the impact of underlying geological structures on yardang morphology (Hu et al. 2017).

Yardang formation is influenced by stratigraphic structures, wind erosion, and fluvial processes. According to Dong et al. (2011), yardang evolution progresses through four distinct stages: embryonic, adolescence, maturation, and recession, each marking significant morphological transformations. Sediment flux in the troughs among yardangs aligns with the hypothesis that wind and wind-blown sediments shape these features over time (Pelletier et al. 2018).

In the Lut desert of Iran, yardangs and their associated corridors are identified and classified by geomorphometric parameters such as slope steepness and curvatures derived from Digital Elevation Models (Ehsani and Quiel, 2008). Further research by Ghodsi (2017) revealed that yardangs in the central and northern regions exhibit greater size and height compared to those in the southern areas, suggesting more advanced stages of erosion and development influenced by both wind and water erosion.

A study in the Dakhla region of southern Morocco highlights the significance of yardangs as paleoclimatic indicators. Field observations and satellite imagery were used to measure the yardangs' length, width, orientation, and density across three 1.5 km² areas (Chahid et al., 2023). The yardangs, ranging from 17 to 467 meters in length and 1 to 7 meters in height and are primarily oriented between 15° NE and 30° NE, differing slightly from the current prevailing wind direction. This analysis provides insights into their development stages and emphasizes their potential as indicators of past environmental conditions (Chahid et al., 2023).

2.1 Yardangs on Other Planetary Bodies

Yardangs are also present across different planetary bodies, highlighting the equifinality of structures that can result from the presence of wind and arid conditions. Planetary yardangs not only reveal insights into current climatic patterns but also provide valuable information about past environmental conditions.

Mars showcases prominent yardang formations in the Gale Crater and Medusae Fossae Formation, indicative of intense aeolian activity and the presence of highly erodible materials. These features suggest sustained arid conditions and complex climatic cycles (Kite et al., 2015; Liu et al., 2020; Kerber et al., in progress). Discrepancies between the Mars General Circulation Model (GCM) predictions and yardang orientations indicate that these features likely formed under ancient wind patterns distinct from those observed today (Greeley et al., 1993).

Titan, Saturn's largest moon, exhibits vast dune fields around its equator, indicating robust wind activity capable of moving materials of various sizes (Lorenz et al., 2006; Radebaugh et al., 2008; Barnes et al., 2015). Titan's surface, covered with sediment from aeolian and fluvial processes derived from organic atmospheric fallout, creates favorable conditions for yardang formation. Yardang candidates identified in Titan's midlatitudes, supported by the erodibility of Titan-relevant materials such as weakly cohesive organic sedimentary rocks, suggest significant aeolian processes shaping its landscape (Paillou et al., 2016; MacKenzie et al., 2023).

The analysis of Titan's surface is challenged by its poor image resolution (300 m). Statistical classifications, based on terrestrial yardang data, were utilized to discern whether straight radar-bright linear features (BLFs) are dunes or yardangs (Northrup, 2018). This model identified yardang-like features based on similarities in sinuosity and spacing with terrestrial yardangs, while other features were determined to be stabilized (Northrup, 2018). The yardangs are large and would thus be mega-yardangs, perhaps remnants of ancient lake basis formed under different climatic conditions (Paillou et al., 2016). This suggests that Titan's midlatitude yardangs may offer a record on its climatic history.

On Venus, yardangs formed in regions marked by volcanic activity and impact

cratering illustrate the dynamic interaction between aeolian erosion and volcanic processes in landscape formation (Khawja et al., 2020; Ganey et al., 2023). Wind streaks associated with parabolic ejecta deposits and observations of yardangs in post-tessera volcanic regions highlight unique erosional processes driven by Venus's dense atmosphere and volcanic activity (Greeley et al., 1995; Khawja et al., 2020).

In-depth studies of Martian yardangs, such as those in the Light-Toned Yardang Unit (LTYu) in Gale Crater, reveal a stratigraphic record of alternating semi-arid to arid conditions. These yardangs are part of ancient erg systems that underwent multiple cycles of deposition and erosion influenced by climatic shifts over millions of years (Dromart et al., 2020). Comparative analyses with terrestrial yardangs in regions like California, Qaidam Basin, China, and the Lut Desert, Iran, provide further insights into their formation and evolution under different environmental conditions (Ding et al., 2020).

Comparative studies of yardangs across Earth, Mars, Titan, and Venus (FIGURE 2) highlight the importance of planetary geomorphology, and aeolian processes in

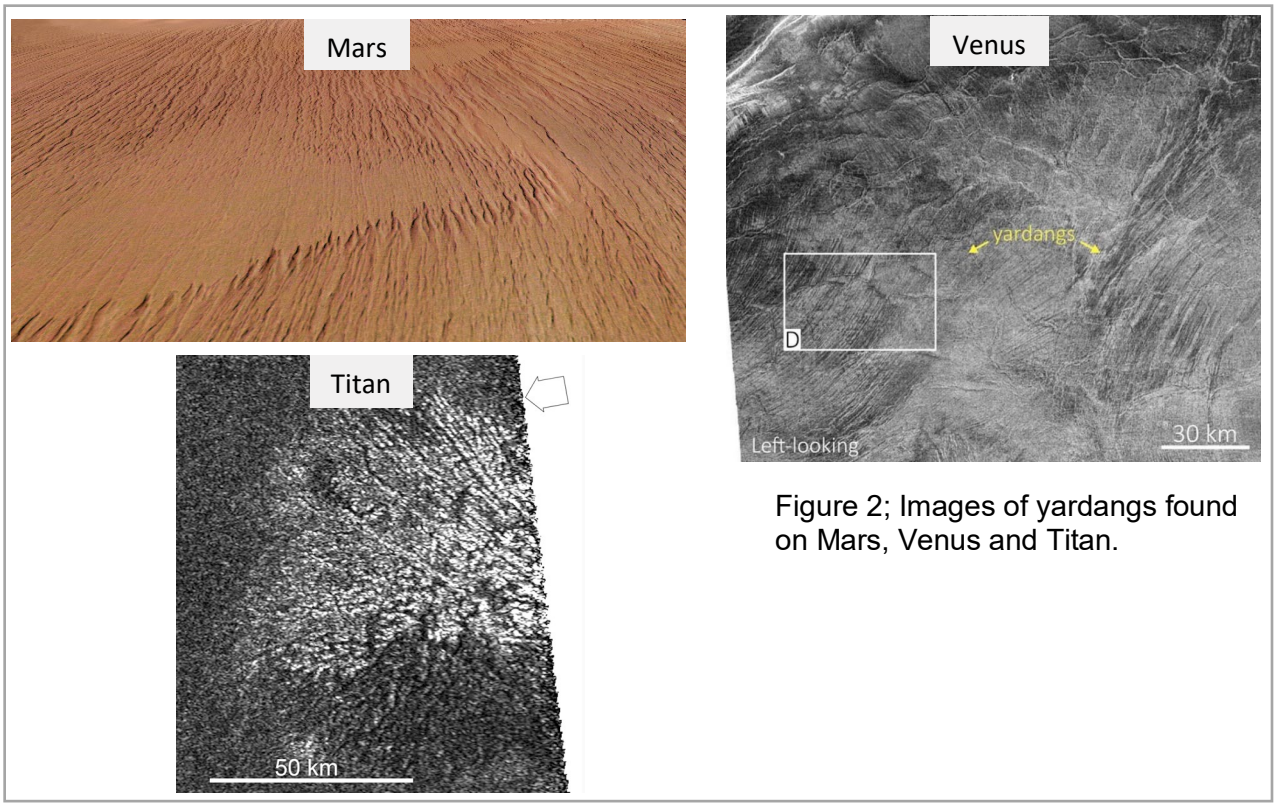

Figure 2; Images of yardangs found on Mars, Venus and Titan.

shaping landscapes. On Mars, yardangs reveal ancient wind patterns and climatic conditions, while Titan's yardangs and dunes suggest significant wind activity and

sediment transport. Venusian yardangs, formed in a volcanically active environment, emphasize the role of wind-driven erosion under different atmospheric conditions. This study's examination of the Puna Plateau's yardangs aims to enrich this global understanding, focusing on their formation, morphology, and evolutionary trajectories.

3 Geological Setting

The Puna-Altiplano Plateau, extending across the Andean regions of Bolivia and Argentina, is characterized by significant geological contrasts. Ranging in elevation from 3,700 to 6,000 meters, the plateau features arid climatic conditions and relatively low regional topographical relief. This high-altitude environment is subject to extreme diurnal temperature variations, low atmospheric pressure, and limited precipitation (Fernandez and Busso, 1999; FIGURE 3).

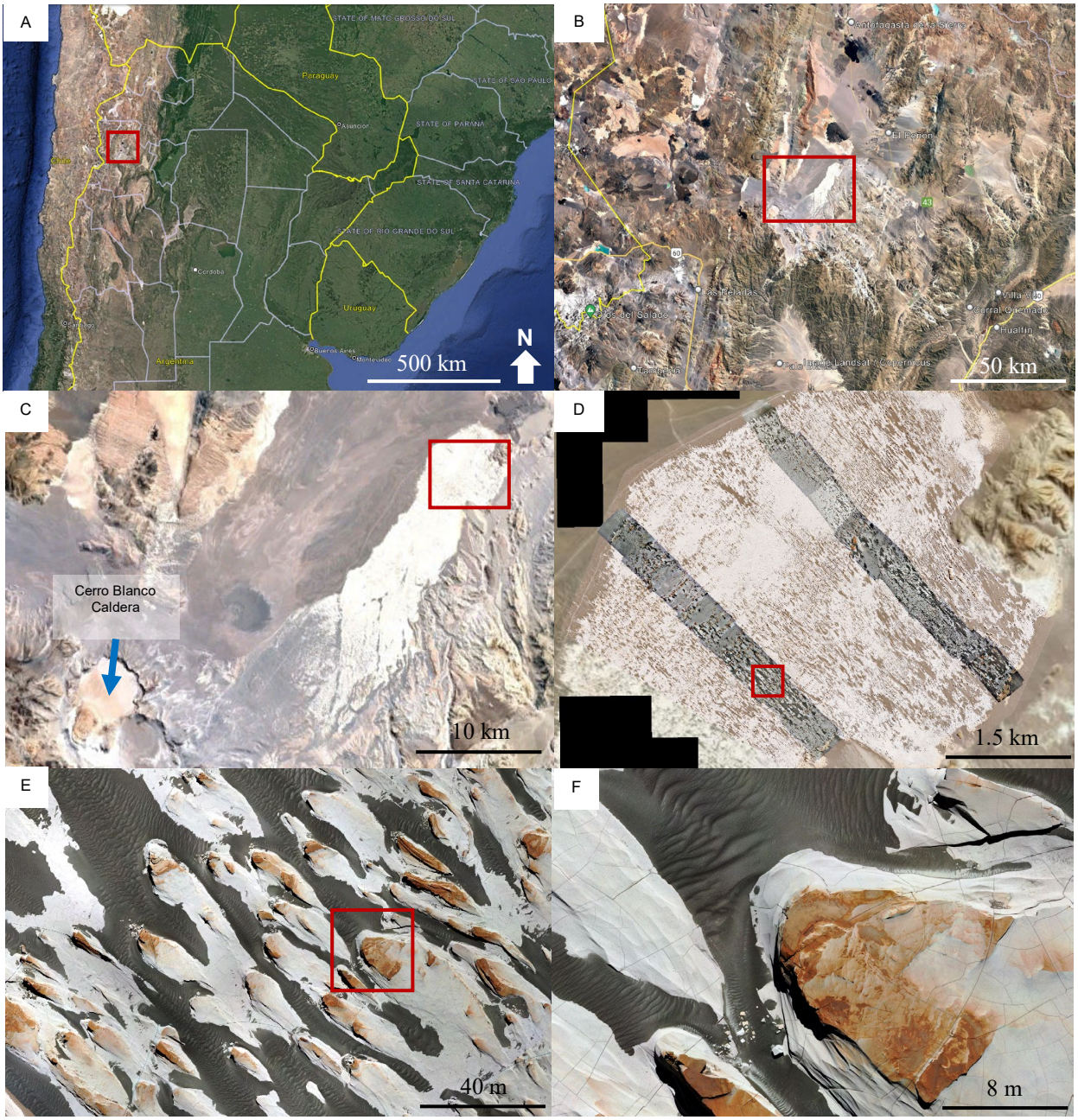

Figure 3; A: Map showing the central portion of South America. B: Map showing a portion of the Puna Plateau in Argentina. C: Map showing the Campo de Piedra Pomez ignimbrite and the Cerro Blanco Caldera from which the ash erupted. D: Upper portion of the CPP showing the study site with satellite and drone imagery. E: Closer section of drone imagery. F: Close up of a yardang from drone imagery, DJI Mavic2 Pro.

Ranked as the second-largest orogenic plateau on Earth, second only to the Tibetan Plateau (Carrapa and Decelles, 2008), the elevated height of the Puna Plateau results from the ongoing subduction of the Nazca plate beneath the South American plate, a geodynamic process that continuously shapes the region's landscape. (Coutand

et al. 2001). This ongoing subduction creates a landscape with young volcanic deposits and semi-indurated ash flows (de Silva et al. 2022). The bedrock supporting the

Figure 4; A 1.73m tall geologist standing at the edge of the Cerro Blanco Caldera 5km wide and walls that reach 300m in height. The caldera is well preserved for an ash flow caldera because of the arid conditions and youth of the feature.

yardangs consists of ignimbrite and Plinian fall deposits from the Cerro Blanco caldera, located on the south flank of the La Hoyada volcanic complex (FIGURE 4). Radiometric dating places these deposits within the timeframe of 70,000 to 55,000 years based on ^{40}Ar-^{39}Ar dating (de Silva et al. 2010).

The yardang fields are predominantly shaped by wind rather than fluvial processes, demonstrating aeolian processes in the plateau's hyper-arid environment (de Silva et al. 2010; Favaro et al. 2021). The prevalence of yardangs in the Puna, particularly within the Campo de Piedra Pomez (CPP) region, offers an opportunity for scientific study, providing a window into how atmospheric forces react with sand and gravel and enact the geological evolution of the bedrock.

Situated within the rain shadow of the Andes Mountains, the region experiences cold and arid conditions, with significant diurnal temperature variations. Despite the extreme conditions, with temperatures ranging from 0 to 10°C and annual precipitation barely exceeding 200 mm (Fernandez and Busso, 2018), the Puna serves as an excellent site for studying aeolian processes. In this environment, aeolian transport mechanisms, especially saltation, dominate the movement of sediments, shaping the landscape's physical characteristics. (de Silva et al., 2010; Favaro et al., 2021).

The winds that sweep across the Puna can reach speeds averaging 100 km/hr and occasionally surpassing 275 km/hr (de Silva et al. 2013). Originating predominantly

from the northwest, going back at least 2 million years (Fernandez and Busso 2018), the persistent winds have sculpted the yardangs into their characteristic whale-back forms, which are evident across the plateau. Evidence of seasonal water or ice is present above the saltation layer in a distinct orange desert varnish – a thin and dark deposit, typically less than 0.1 mm thick (Goldsmith et al. 2014; Sarmast et al. 2017). The orange-stained yardang tops contrast starkly with the dark grey gravels and the white ignimbrite bedrock, which contains clear quartz and other ash-related lithics, also light in color (de Silva et al. 2010; Baez et al. 2020; McDougall, 2022; FIGURE 5). The

Figure 5; Showing the contrast between yardangs (elevated landform with orange tops), gravel (dark grey) and bedrock (white).

distinct geological and climatic conditions of the Puna-Altiplano Plateau set the stage for a detailed exploration of yardang formation and evolution, as discussed in the subsequent sections

4 Yardangs in the Puna and Previous Work

This study focuses on yardangs sculpted into the ignimbrite formations of the Campo de Piedra Pomez (CPP), a region that has become a focal point in geomorphological research. Other studies have also focused on the yardangs in this region. McDougall (2022) conducted an extensive morphometric analysis of CPP yardangs, emphasizing the characteristics of the ignimbrite substrate and their influence on yardang morphology. This research introduced a semi-automated technique to

quantify yardang parameters such as shape, orientation, spacing and curvature, providing a detailed understanding of the landform shapes in the region. Additionally, McDougall's fieldwork included sample collection to analyze the density, porosity, and structural integrity of the ignimbrite, laying groundwork for further exploration into the material properties influencing yardang formation.

Concurrently with McDougall, Kerber et al. (in progress) explored yardang formation through aeolian processes, proposing that yardangs evolve not from existing protrusions but through the erosional reduction of the areas between them. Their research suggests that yardangs do not start from pre-existing protrusions (FIGURE 6) but are remnants of interyardang areas eroded away by abrasion, deflation, and

Figure 6; Low angle drone picture showing direction and shape of yardangs, along with gravel, and bedrock with a person for scale.

saltation. While other studies, such as Dong et al. (2012), de Silva et al. (2010), and Pelletier et al. (2018), propose additional factors like flooding, mass wasting, and rain in yardang formation, these factors are unlikely to have influenced the CPP due to its arid environment. Key questions persist regarding the initial formation process, the possible preferred substrate age, and the temporal persistence of these features until complete

erosion. Addressing these queries promises enhanced predictive capabilities concerning the formation of yardangs on Earth and other planets.

Another study focused on the properties of the ignimbrite. In the Central Andes, ignimbrites are categorized into hard and jointed, and soft with ash and pumice. The harder rock forms tall ridges with steep sides and elongated tails, while the soft rock erodes more easily, forming smaller and shorter ridges. Such differences in substrate hardness not only dictate yardang morphology on Earth but also offer insights into similar formations, like Mars' Medusae Fossae Formation (de Silva et al. 2010).

Building on previous studies of yardang formation in the CPP, Favaro et al. (2021) identified that yardangs in this region are not randomly scattered but frequently organize into clusters or bands across the landscape. These bands are aligned transverse to the prevailing northwest winds, suggesting a strong influence of both wind direction and antecedent topographic features, such as ridges and fumaroles, on yardang distribution and formation. This spatial organization supports the hypothesis that pre-existing topography plays a significant role in the development and alignment of yardangs in the CPP, adding another layer of complexity to the understanding of aeolian processes in this region.

Building upon McDougall's (2022) work, this study employs advanced drone imagery techniques to further delineate yardang morphology and distribution across a broader area of the CPP. It extends the analysis across a broader transect of the CPP incorporating drone imagery captured during December 2019 (FIGURE 7) and March

Figure 7; Original drone imagery transect. The drone imagery is shown as the darker and higher resolution imagery on top of the lighter satellite imagery. The satellite imagery is on top of low-resolution Google Earth imagery. Wind direction is from northwest to southeast.

2024 field seasons. However, this study's approach focuses on the relative distribution of yardangs, gravels, and substrate and how patterns in this distribution reveal aspects of yardang formation.

Yardangs are shaped by a combination of geological structures, wind dynamics, and sediment transport mechanisms. The interplay between these factors results in diverse yardang morphologies observed across different deserts on Earth and other planets. Yet, questions still linger regarding their genesis, the factors that dictate their longevity, and their broader implications for terrestrial and extraterrestrial landscapes.

Investigating yardang formation enhances our understanding of terrestrial geomorphology and provides valuable analogs for deciphering aeolian processes on other planetary bodies. Armed with these insights from previous studies, the following sections detail new analytical findings that not only confirm some established theories but also introduce novel perspectives on yardang development in the CPP

5 Research Methods

This study aims to analyze the distribution, morphology, and formation processes of yardangs in the Campo de Piedra Pomez (CPP) region of the Puna, employing advanced imaging and analytical techniques. This involved detailed data collection using drone and satellite imagery, as well as the application of photogrammetric techniques to create high-resolution orthomosaics and Digital Elevation Models (DEMs). Additionally, the study aimed to understand the relationship between yardang formation and the surrounding gravel distribution by conducting a comparative analysis of the collected samples.

High-resolution drone imagery was captured (FIGURE 8) using DJI Mavic2 and

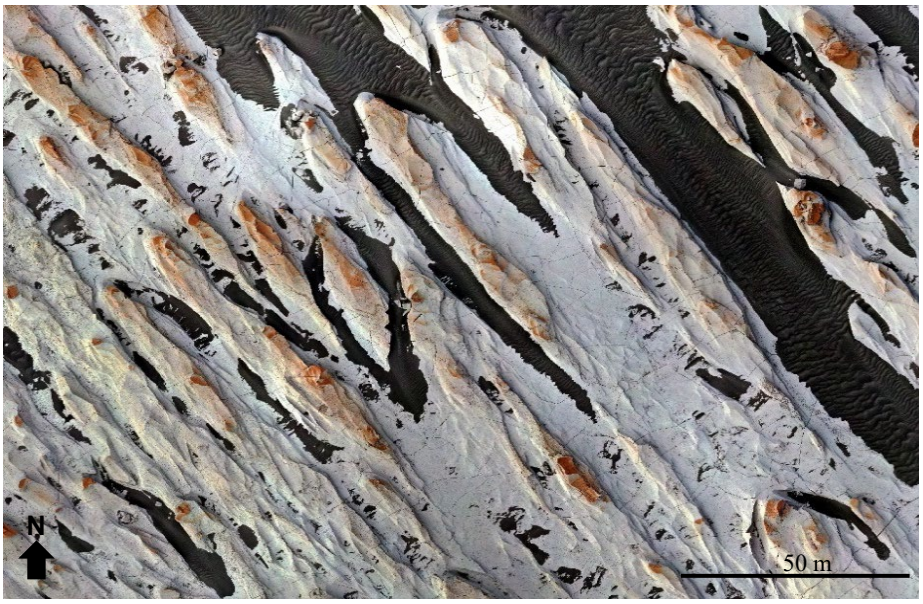

Figure 8; Section of an orthomosaic raster, created from DJI Mavic2 Pro drone imagery captured in the Campo de Piedra

Mavic2 Pro drones during the 2019 and 2024 fieldwork campaigns, providing detailed visual data for analysis. During the 2019 field campaign, thousands of images were obtained over an area of 6 km by 0.5 km at an altitude of 100 m, resulting in a resolution

of 3cm. A total of 8 images passes were completed with each containing 250-350 images, typically corresponding to a single battery life for the drone. In the 2024 field campaign, a similar number of images 2 km southwest of the 2019 site were collected, covering an area, this time, of 5 km by 0.5 km due to increased image overlap, maintaining the same 3 cm resolution (FIGURE 9). Using Agisoft Metashape, each set of drone-captured images was processed to create comprehensive orthomosaics and detailed Digital Elevation Models (DEMs).

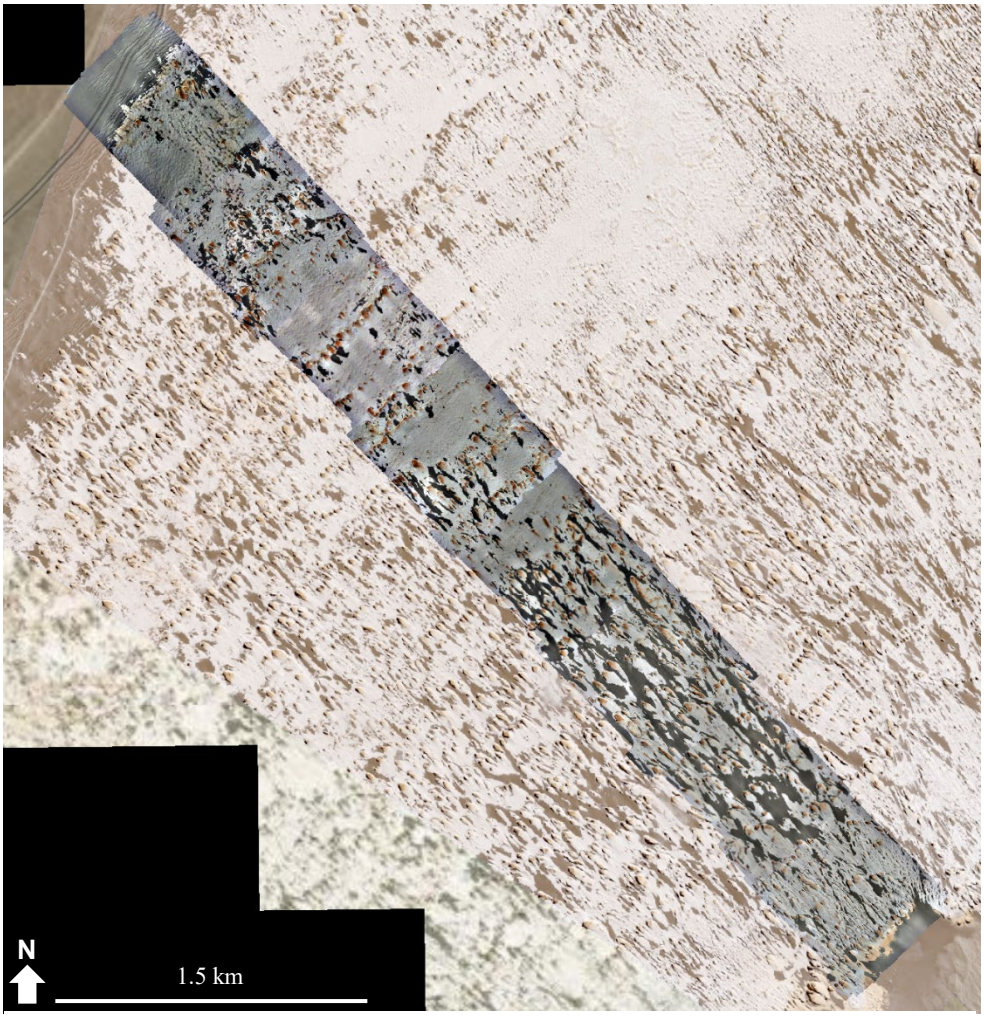

Figure 9; New drone imagery transect. The drone imagery is shown as the darker and higher resolution imagery on top of the lighter satellite imagery. The satellite imagery is on top of low-resolution Google Earth imagery with the black shapes being relicts from the satellite imagery. Wind direction is from northwest to southeast.

Satellite imagery (PNEO “HD15” RGB; FIGURE 10) was obtained from LAND INFO Worldwide Mapping LLC, covering two sections of 25 km^2 and 100 km^2 with a

Figure 10; Two satellite imageries with 15 cm resolution on top of low-resolution Google Earth imagery. Both collected in May 2023. Acquired from LAND INFO Worldwide Mapping LLC. Wind direction is from northwest to southeast.

resolution of 15 cm. The significant resolution differences between the drone and satellite imagery influenced the study's results, which are discussed in more detail below. Samples of the gravel were also collected throughout the field to compare the size, shape, and composition to see if a pattern would reveal another aspect of possible yardang formation.

In this study, the application of photogrammetric techniques was instrumental in capturing the intricate topography of the meso-yardangs within the CPP region of the Puna. Photogrammetry is the process of using photographs to create digital models representing the physical world. This method offers a versatile toolkit for terrain measurement and analysis through the integration of handheld, airborne, or spaceborne

imagery. As explained by Villarreal et al. (2022), photogrammetry serves as a conduit for extracting parameters such as morphology, dimensions, and positioning, thereby laying the foundation for spatial analysis.

The initial stage of data processing involved the creation of orthomosaics and Digital Elevation Models (DEMs) with a spatial resolution of 3cm. This process, facilitated by the DroneDeploy and Agisoft Metashape software, allowed for stitching of individual images into a single orthomosaic. The DroneDeploy software enables the user to set an appropriate distance from the ground, which allows automatic image capture and consistent image resolution (Villarreal et al. 2022).

The Structure from Motion (SfM) technique, implemented through Agisoft Metashape, aligns multiple images to construct a unified 3D spatial representation, using both camera position/orientation and onboard GPS data for precise georeferencing without the need for ground control points (Turner et al. 2012).

The process for stitching the images together is as follows: Upload the images into Agisoft Metashape and select align images. Following the alignment of images, a sparse cloud was generated effectively representing each image as a point within a 3D space. This step facilitates the identification and removal of any stray points in the x, y, z dimensions that could adversely impact the final output. Subsequently, an overall image mask is generated providing finer control over the selection of points. By scaling the image to fit within the confines defined by Agisoft, the mask retains only those points falling within this boundary, eliminating any outliers. This automated process often proves more efficient than manual removal of stray points. With the mask imported, the next phase involves creating a dense cloud, characterized by significantly higher point density, thereby enhancing spatial resolution (FIGURE 11). Upon completion of the dense cloud, the software proceeds to generate the final products: an orthomosaic—a composite image stitched together from multiple images—and a Digital Elevation Model (DEM) (FIGURE 12) derived from the drone's altitude during image capture.

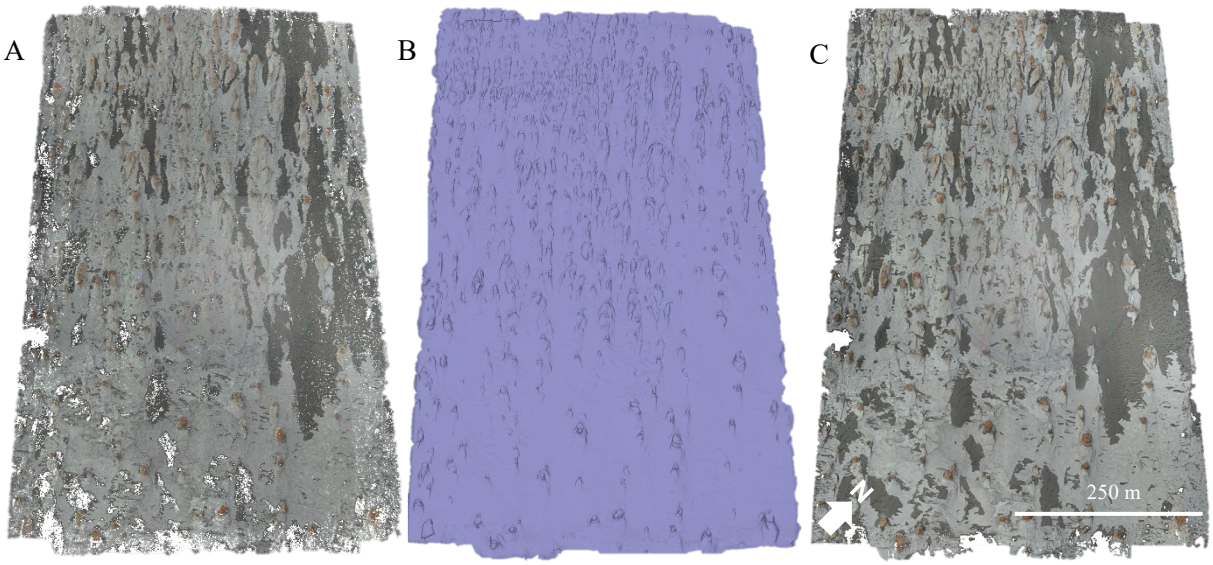

Figure 11; Agisoft Metashape images A: Sparse cloud image showing lots of small points with holes in the imagery where there was less data. B: Mask of the sparse cloud image which helps to remove stray points. C: Dense cloud image showing even more small points that fill in the image more making it look like it is one image.

Following image processing, the orthomosaic raster images were classified using ArcGIS Pro, leveraging its spatial analysis capabilities to distinguish between yardangs, gravel, and bedrock. Distinct features within the imagery, including yardangs, gravel, and bedrock, were delineated using the Image Classification tool, based on predetermined criteria and spectral signatures. This process facilitated the extraction of insights regarding the spatial distribution and composition of these features, laying the groundwork for further analysis.

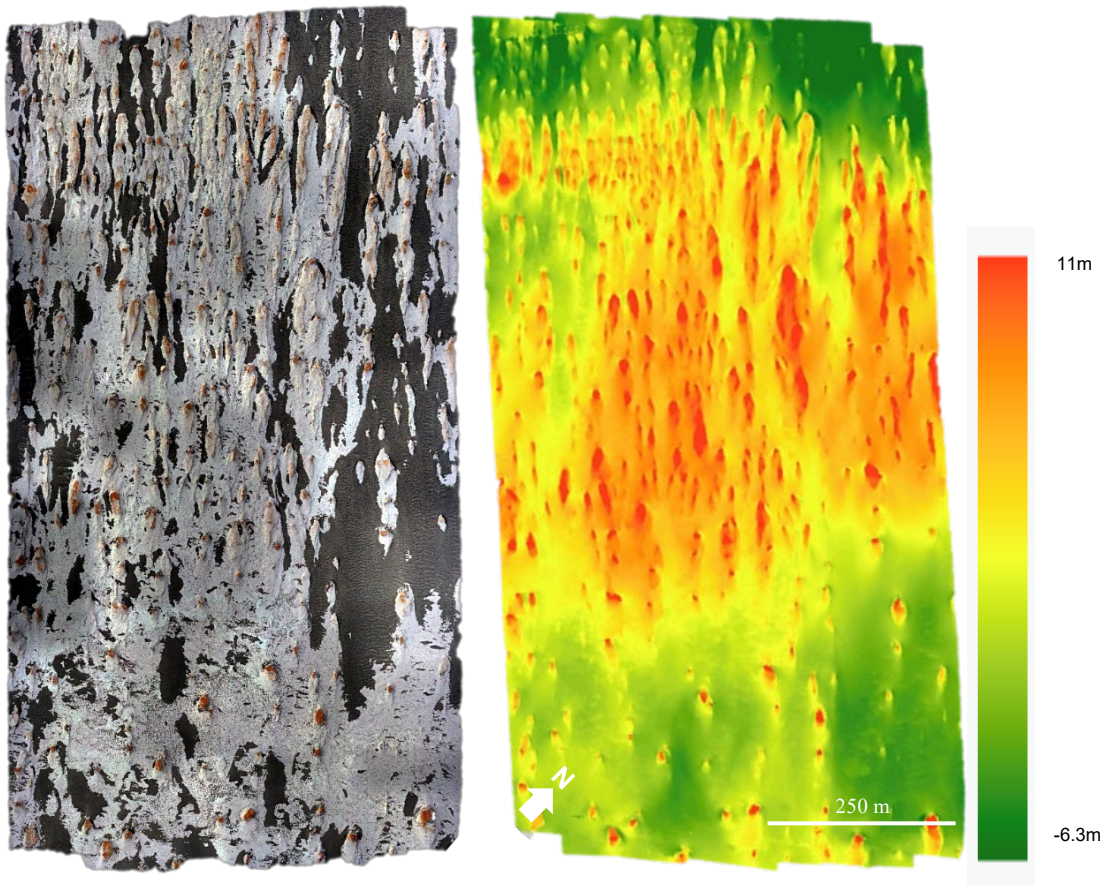

Figure 12; Orthomosaic (left) and Digital Elevation Model (right) with green being lower elevation and red being higher elevation.

The first step is to create a segmented image (FIGURE 13), which is a raster

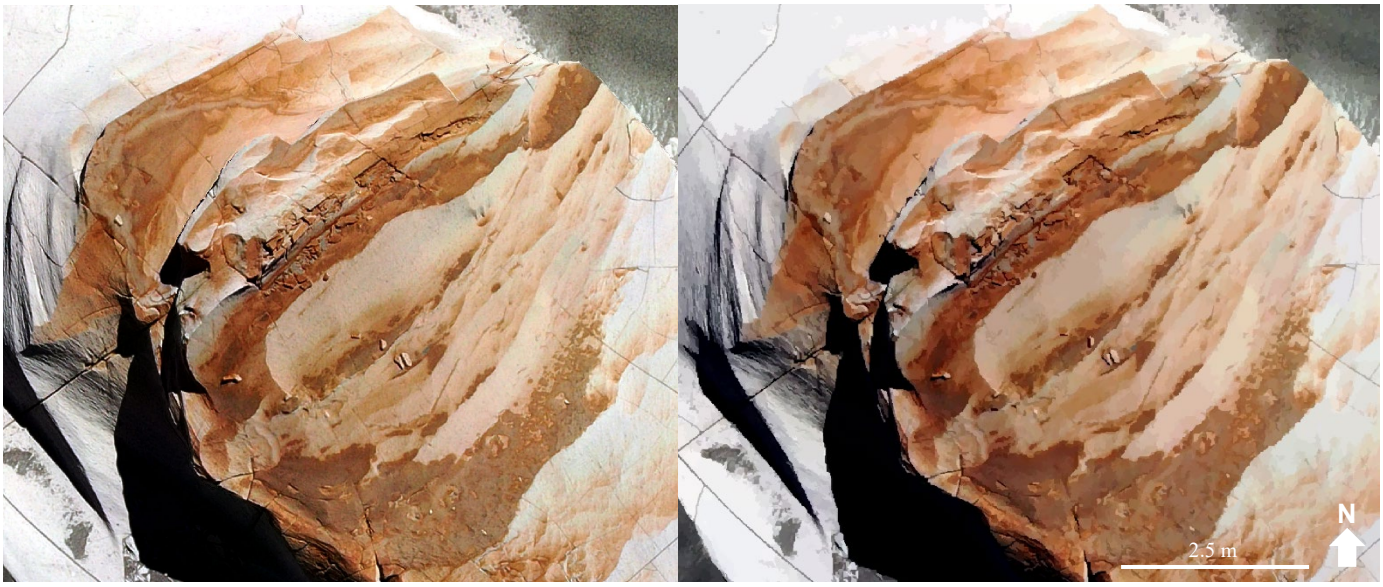

Figure 13; Zoomed in orthomosaic of a yardang (left) and segmented image, where similar pixel colors are grouped together (right).

image that has been processed to group pixels into meaningful regions, or segments, based on their spectral, spatial, and textural properties. This image segmentation process uses algorithms to analyze pixel values and group adjacent pixels with similar characteristics, transforming the raster into a more understandable and analyzable format. Users can adjust parameters like spectral, how similar the objects you want to identify are, and spatial, how clustered together the objects you want to identify are, detail, with numbers from 1 (low) - 20 (high), to control the segments' size, shape, and compactness. This allows analysts to extract and interpret meaningful information from complex raster datasets more accurately and efficiently. For this study, a spectral number of 20 and a spatial number of 15.5 was used. These numbers were determined by hand drawing polygons around the objects to be identified, within a small portion of the image (FIGURE 14) and comparing several iterations of different spectral and spatial numbers to the hand drawn results. The option that was most accurate returned values at about 82% accuracy to the hand-drawn image.

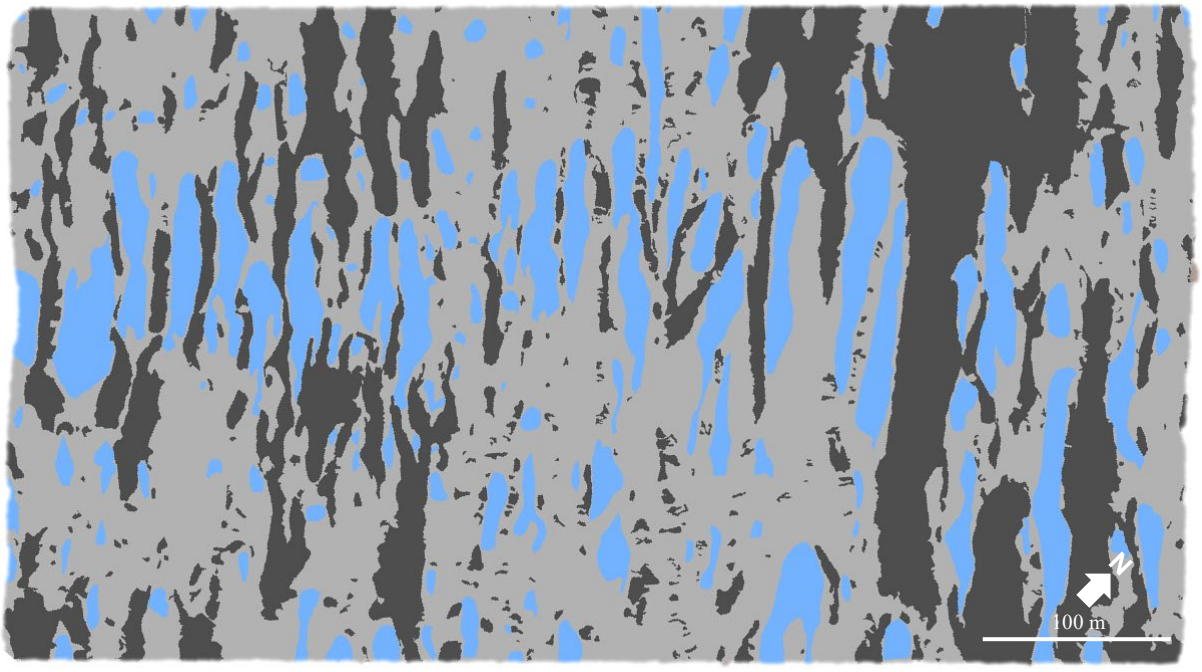

Figure 14; Hand-drawn map of yardangs (blue), gravel (dark gray), and bedrock (light gray). Used to compare accuracy with computer classification.

After the segmented image is created, the Training Samples Manager is used to create a schema based on the objects to be identified and the color to be assigned to

each object. During this step, three classes were identified as points of interest to be classified in each orthomosaic image: yardangs, gravel, and bedrock. These classes were chosen due to the strong contrast between them, resulting from differences in geological origin and processes on each feature, which are the focus of delineation. Most yardangs have an orange, oxidized, top while the gravel is dark grey, and the bedrock is white. These differences in color create a high degree of accuracy in classification.

The next step is to use the Training Samples Manager in ArcGIS Pro to train the dataset. This step enables the user to create a classification system out of the features to be identified and then create polygons by hand to capture the pixel values of each object. Over 150 samples of each of the three features (bedrock, gravel, yardangs) (FIGURE 15) were collected to give the tool enough information to calculate an accurate

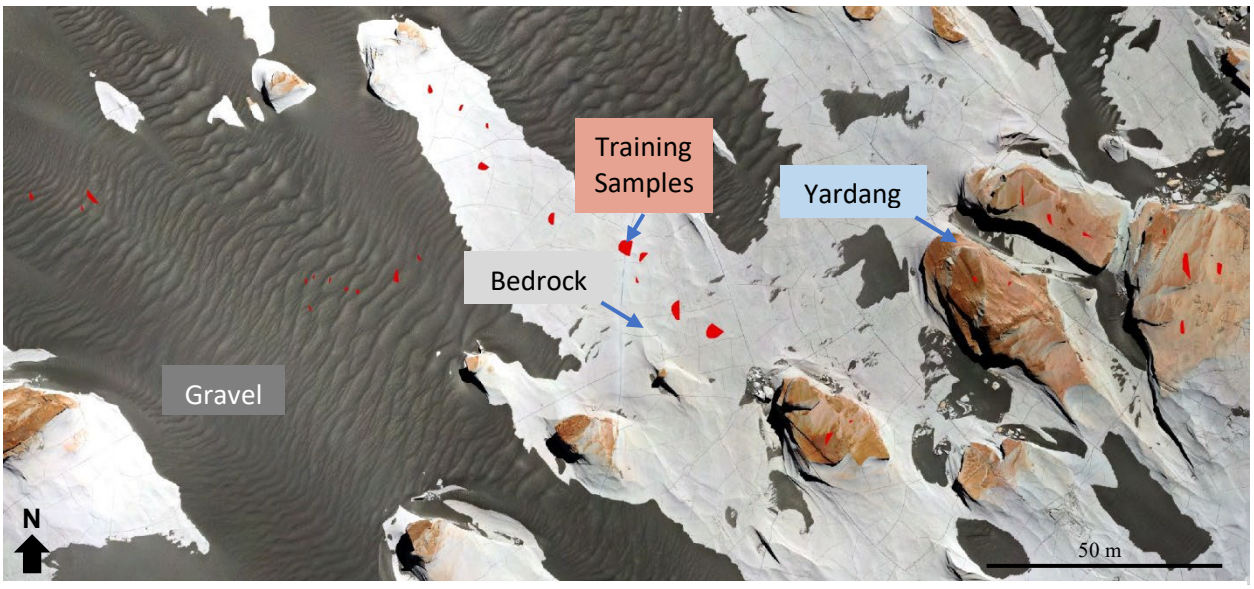

Figure 15; Training samples, shown as red polygons, capturing the three classes of gravel, bedrock, and yardang.

classification image. After inputting the segmented image and the training samples, the tool is run and will use the samples to produce a new raster containing only the three features classified under the identified categories (FIGURE 16). The new raster was then analyzed by turning the classes into polygons to extract the area and distribution of each. These areas were then compared to find the percentage that each class occupied within the image. MATLAB was used to create plots (FIGURE 17) that horizontally scan

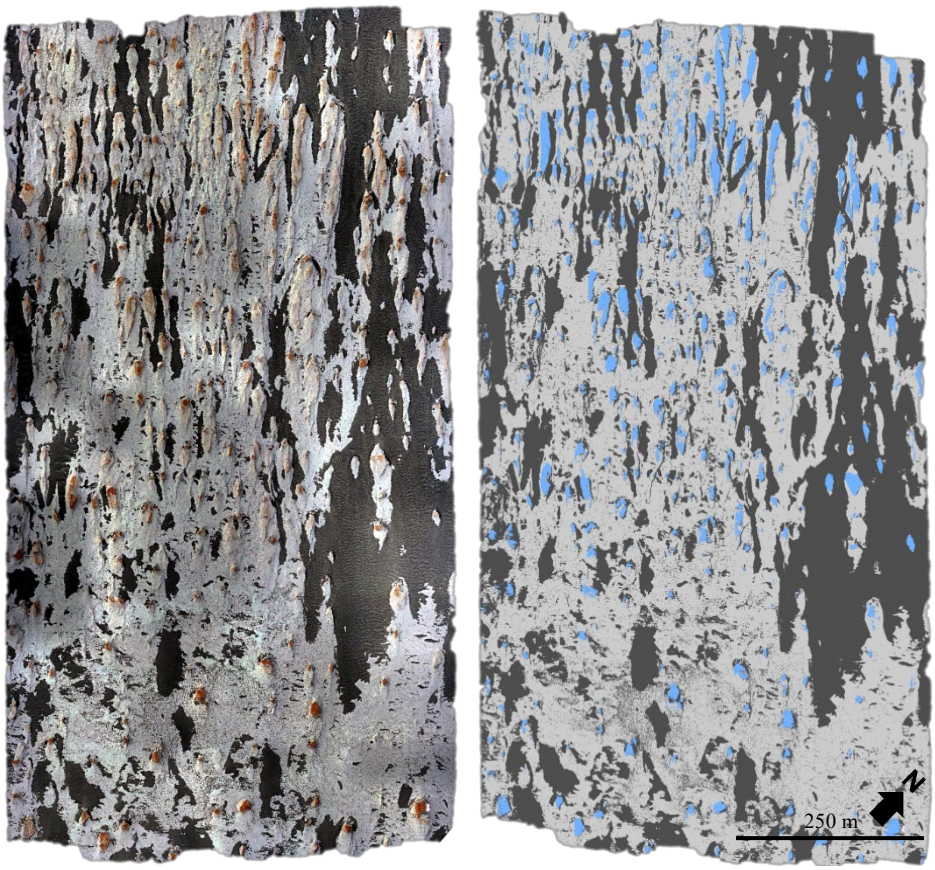

Figure 16; Orthomosaic image (left) and Classified image (right):
Blue = Yardangs,
Dark Gray = Gravel
Light Gray = Bedrock

the classified satellite imagery from upwind to downwind and produces plots of relative material abundances.

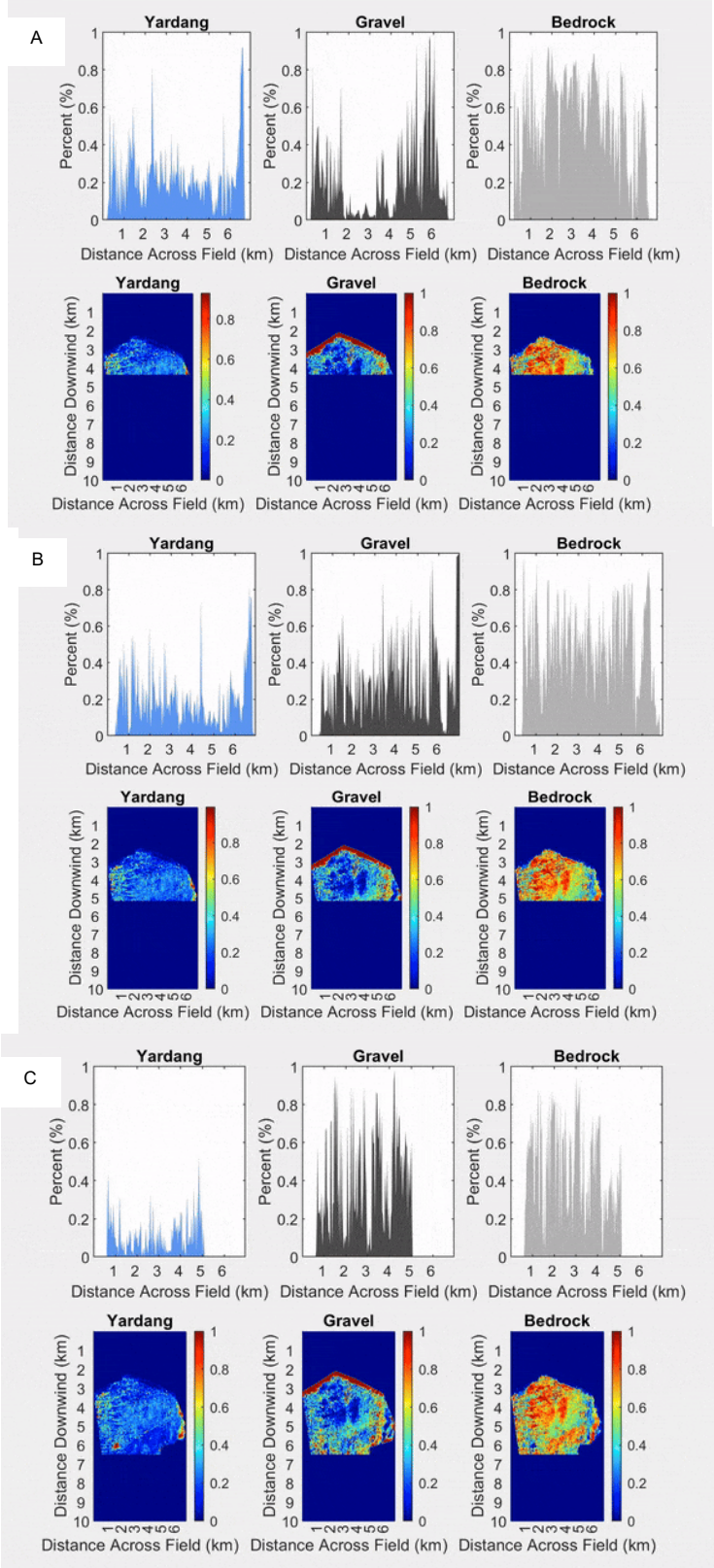

Figure 17; Classified, upper, portion of satellite imagery depicting proportions of yardangs, gravel, and bedrock moving from upwind to downwind. Location (A), upwind where there is a higher proportion of yardangs and bedrock with a lower proportion of gravels. Location (B), middle of the field where there begins to be an increase in gravels and decrease in yardangs and bedrock. Location (C), downwind where yardangs and bedrock proportions are significantly lower, and the gravel proportion is significantly higher.

The high-resolution drone imagery (3 cm) captures intricate aspects of the geology and topography. In contrast, the satellite imagery, with a resolution of 15 cm,

while effective for broader classifications, offers a less detailed perspective (FIGURE 18). This difference in resolution (FIGURE 19) impacts the precision of the classification analysis. For instance, smaller yardangs and finer morphological details are accurately identified in the drone imagery but appear less distinct or even indistinguishable in the satellite imagery (FIGURE 20). Consequently, while both data sources are valuable, the classifications derived from each must be interpreted with an understanding of their respective resolution limitations. Additionally, the time of day the satellite imagery was captured can affect the presence of shadows, as seen in the 25 km² satellite imagery. These shadows complicate classification, as they are often misclassified as gravel, thereby altering the gravel proportion in the statistical analysis.

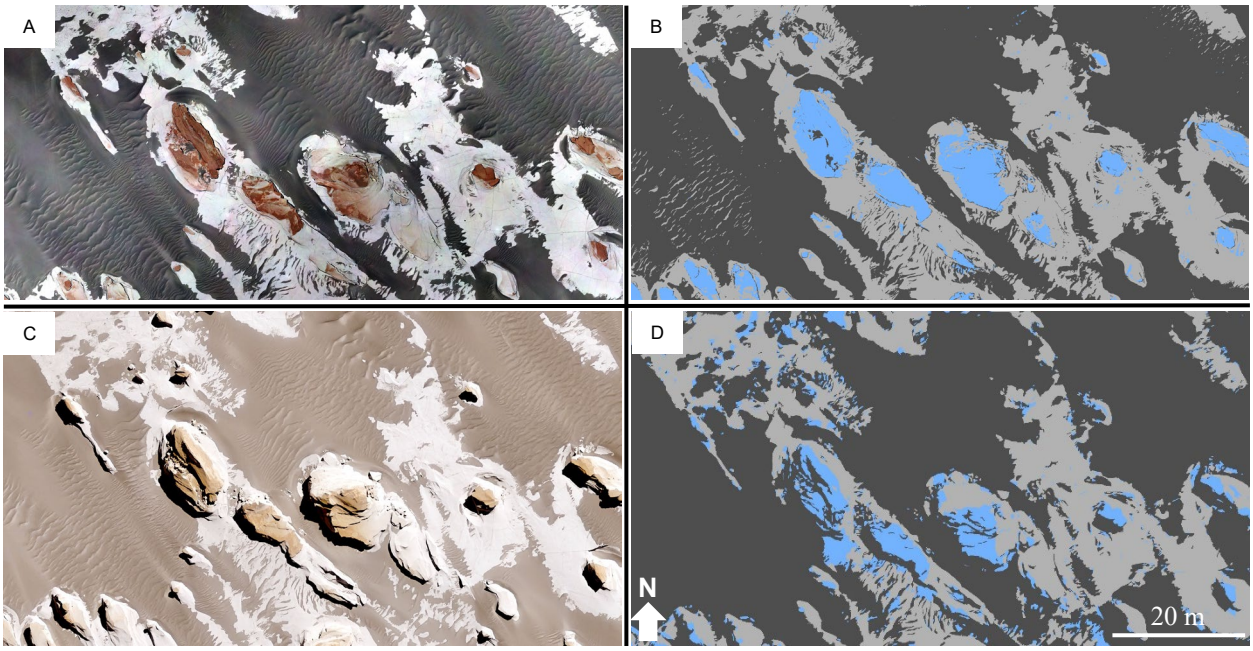

Figure 18; A: Drone imagery (3cm). B: Drone imagery classification showing that the tops of some gravel ripples' tops were misclassified as bedrock. It also shows that it classified the yardangs a lot more accurately than the satellite imagery's classification. C: Satellite imagery (15cm). D: Satellite imagery classification showing the misclassification of shadows as gravel and less accurate yardang classification.

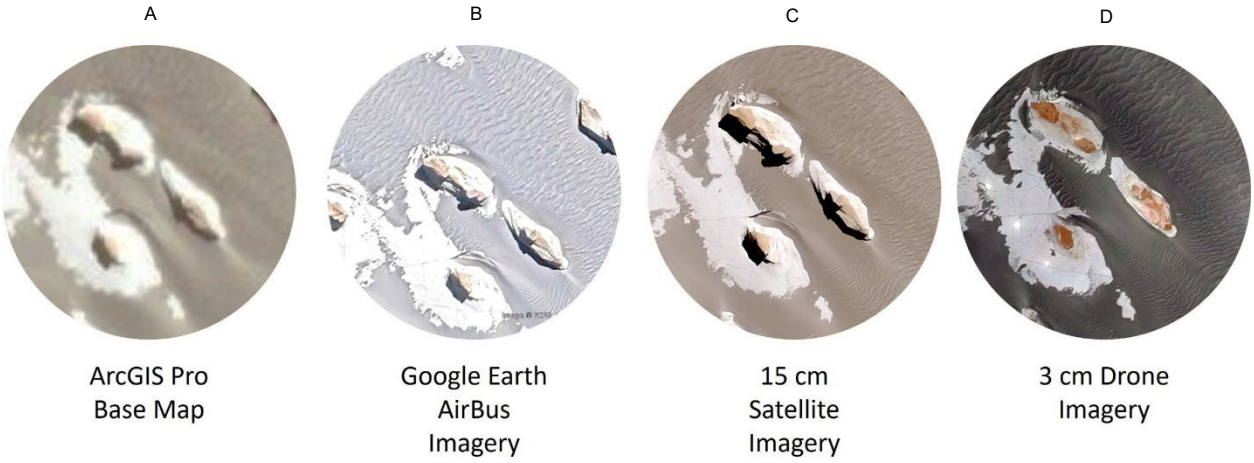

Figure 19; Different image resolutions for the same location.

The Digital Elevation Models (DEMs) showed an expected general regional slope (Favaro et al., 2021) in the area. That regional slope was removed to better show the elevation differences of the yardangs compared to the bedrock. About 5,000 random points were created within a polygon fit over the DEM, then, the elevation data from the DEM was extracted to the points and a trend analysis completed to create a raster of the average slope. This tool uses a global polynomial interpolation that fits a smooth

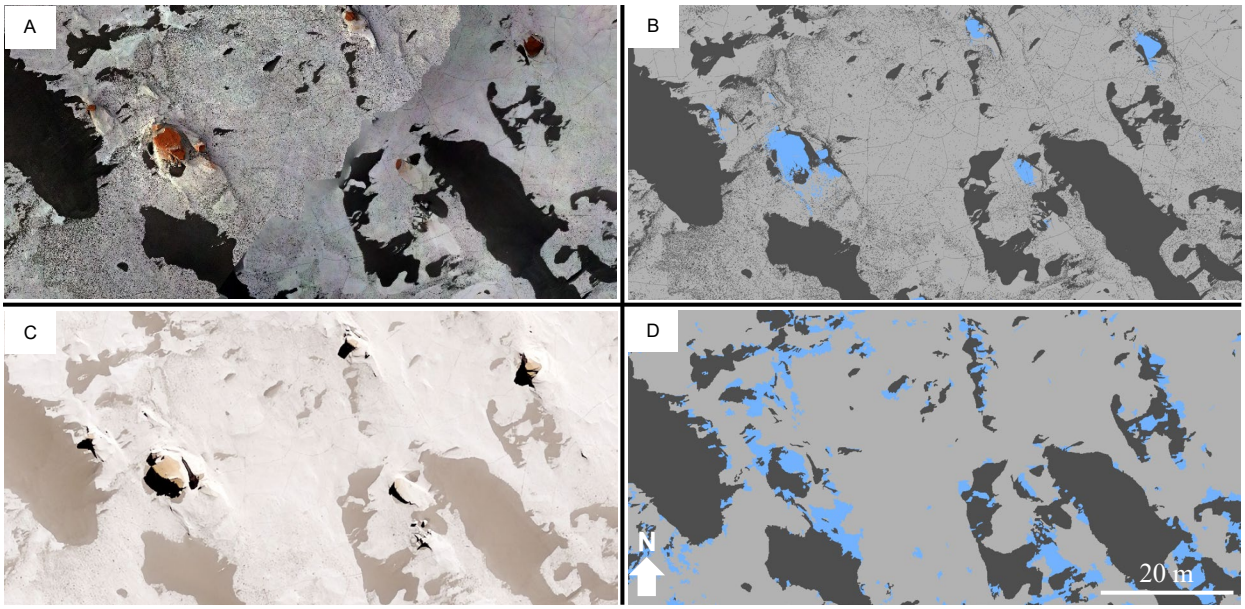

Figure 20; A: Drone imagery (3cm). B: Drone imagery classification showing the details that the classification process revealed like the small pits of gravel and the cracks in the bedrock. C: Satellite imagery (15cm). D: Satellite imagery classification showing the lack of detail viewed because of lower resolution and more even image tones. It also shows the lower accuracy of classifying the yardangs.

surface, defined by a polynomial function, to the input sample points. The trend raster was then subtracted from the DEM to obtain the slope-removed DEM (FIGURE 21).

In 2024, drone imagery was recaptured at the same location as in 2019 to facilitate a detailed change detection analysis, comparing temporal differences in landscape features (FIGURE 22). This involved aligning the 2024 orthomosaic with the 2019 orthomosaic and using image differencing techniques to quantify changes in the imagery over the five-year period. This analysis was facilitated by ArcGIS Pro, where both raster images were compared to detect and measure changes in the gravels. The comprehensive methodologies employed, from high-resolution drone imaging to GIS analyses, ensure an investigation of yardang dynamics, paving the way for detailed results and discussions in the subsequent sections.

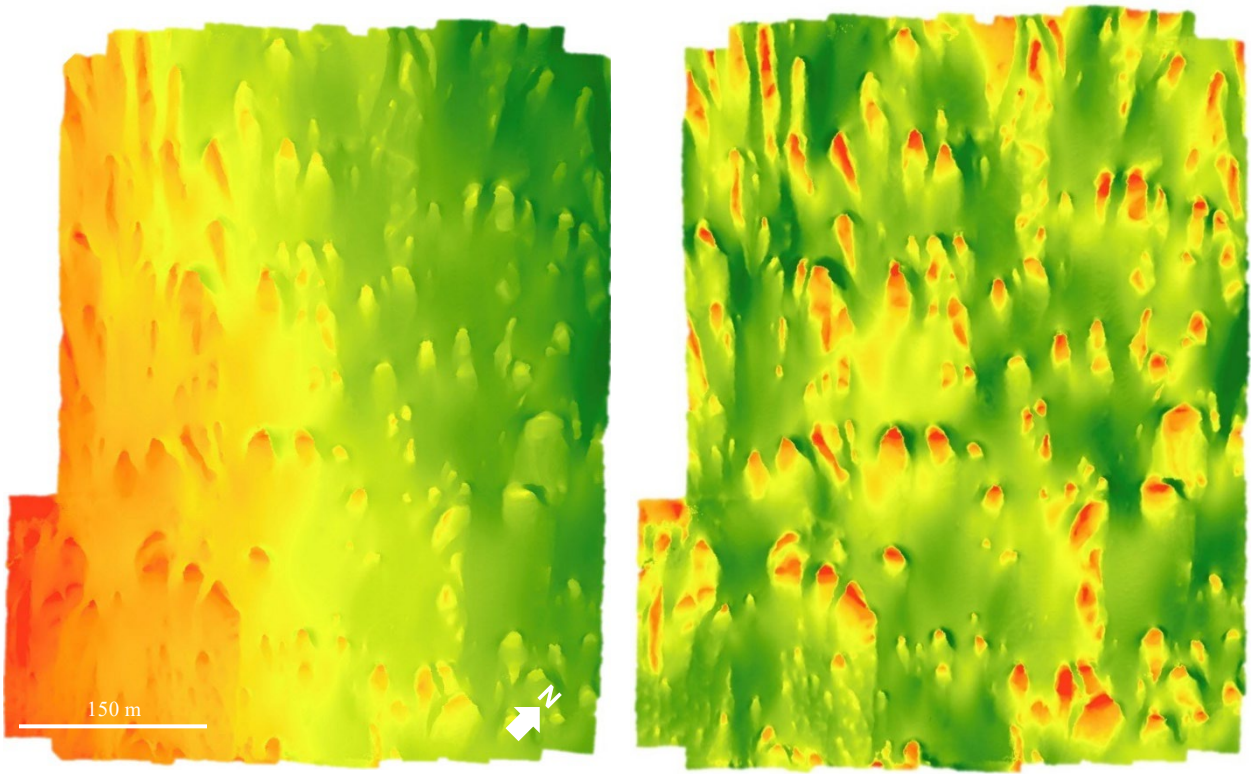

Figure 21; Original Digital Elevation Model (left) showing the general regional slope where it is higher to the left and lower to the right. Slope-fixed Digital Elevation Model (right) showing the pronounced and higher yardangs in relation the lower surrounding area. The regional slope was removed to better show the elevation differences of the yardangs compared to the

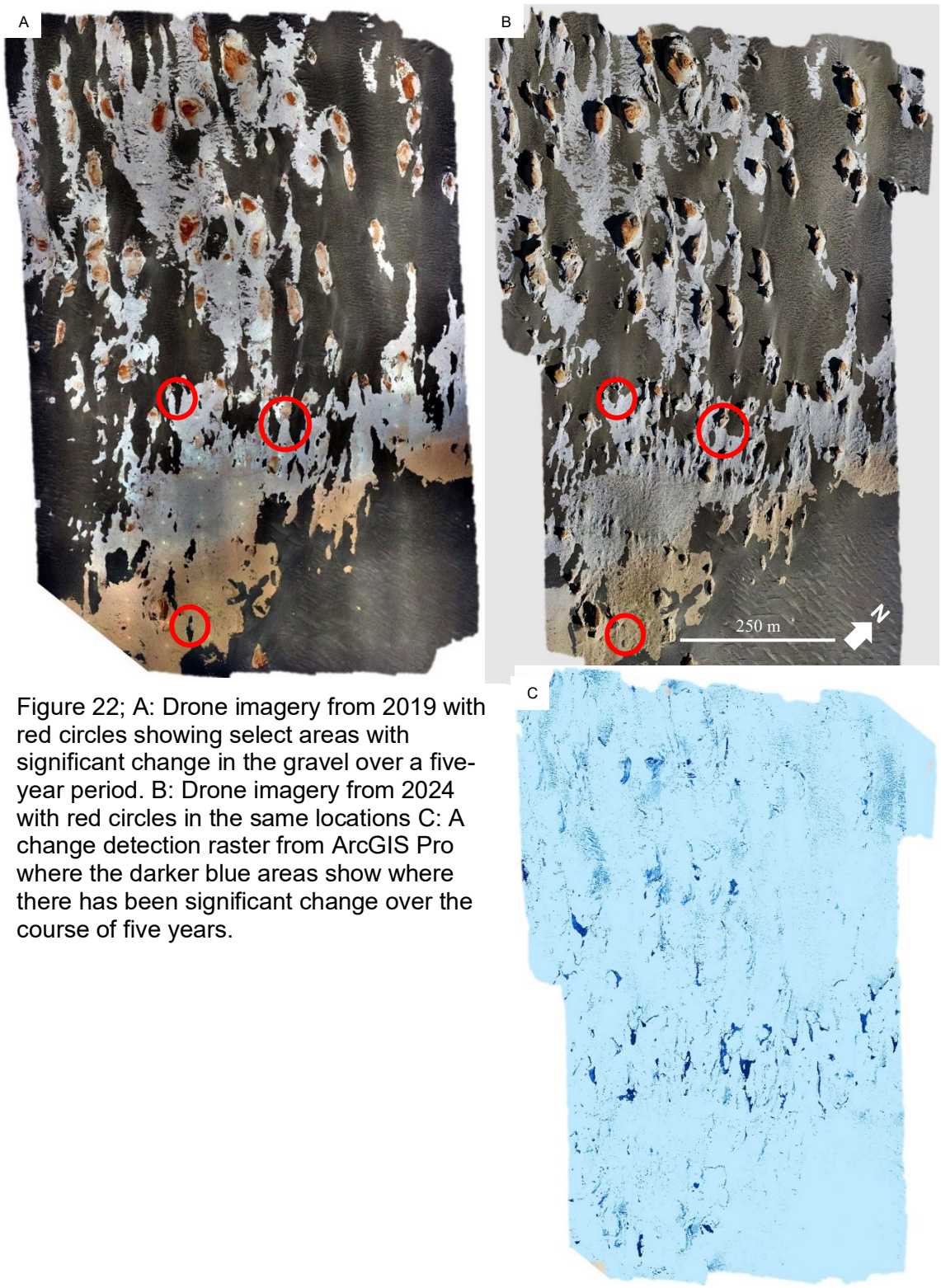

Figure 22; A: Drone imagery from 2019 with red circles showing select areas with significant change in the gravel over a five-year period. B: Drone imagery from 2024 with red circles in the same locations C: A change detection raster from ArcGIS Pro where the darker blue areas show where there has been significant change over the course of five years.

6 Results: Yardang, Gravel and Bedrock Distribution across the Puna

The classification analysis yielded new insights into the spatial dynamics of yardang distribution within the study region. Across the CPP, a consistent pattern was

identified from the northwest (front of the field, or windward side) to the southeast (downwind side). Notably, the total yardang and bedrock area decreased, while gravel coverage increased, all exhibiting a roughly linear pattern (FIGURE 23).

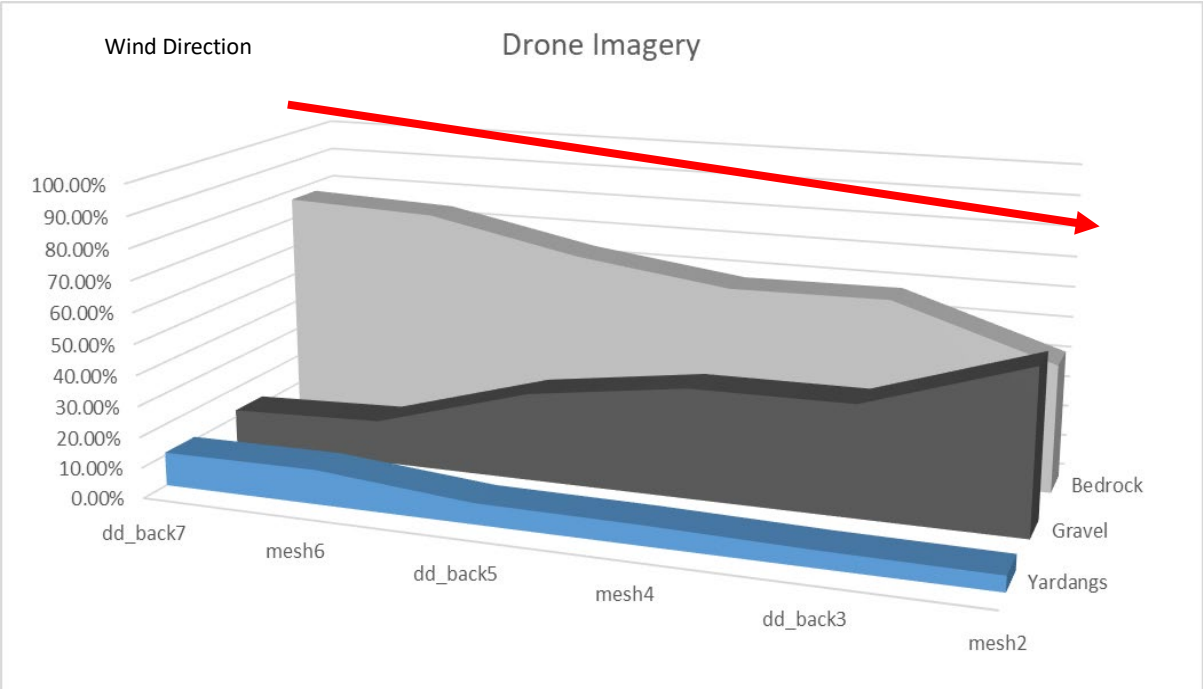

Figure 23; Chart showing the pattern of decreasing percentage of yardangs and bedrock and increased percentage of gravel traveling from upwind to downwind.

MATLAB-generated plots clearly illustrate these trends, mapping the percentage coverage and distribution of yardang, gravel, and bedrock materials across the field (FIGURE 17). The plots demonstrate the horizontal scanning of the classified satellite imagery from upwind to downwind, illustrating the relative material abundances of yardang, gravel, and bedrock. The top row of plots shows the percentage coverage of each material across the field. The yardang, gravel and bedrock plots reveal significant variation in abundance across the field, with yardang and bedrock abundances decreasing and gravel abundance increasing from upwind to downwind. The bottom row of heatmaps provides a visual representation of the relative abundances of each material. The heatmap indicates the percentage of yardangs, gravel and bedrock present, with the most intense colors representing the highest concentrations.

These plots show a clear trend where the yardang and bedrock coverage decrease while gravel coverage increases from windward to leeward. This pattern is indicative of active aeolian processes where wind erosion gradually reduces the

exposed bedrock and yardangs, redistributing the material and gravel downwind. The observed increase in gravel concentration downwind suggests ongoing sediment transport and deposition, which plays a crucial role in the evolution and maturation of the yardangs. Understanding these changes in concentration is essential for setting up the staged progression model, as it highlights the continuous interaction between erosional forces and sediment dynamics that shape the landscape over time.

The change detection analysis between the 2019 and 2024 orthomosaics (FIGURE 22) revealed stability in yardang structures but noticeable fluctuations in gravel distribution. These findings imply that yardang weathering does not occur on a short timescale (years to decades), whereas gravel areas exhibit year-to-year changes, controlled by prevailing wind conditions and sediment transport dynamics observed during the study period. Specifically, hand-drawn polygons identified areas of gravel presence and absence (FIGURE 24), revealing that gravel currently present in 2024 but not in 2019 covers 3926.3 m^2, while gravel present in 2019 but not in 2024 covers 3736.0 m^2. The similarity in these numbers suggests a potential continuous exchange of gravel. Estimated gravel movement volumes range from 39.3 m^3 for a 1 cm depth to as

Figure 24; Orthomosaic from 2024 showing areas (green) where there was no gravel in 2019 but is currently present and areas (red) where there was gravel in 2019 but is not currently present.

much as 117.8 m³ for a 3 cm depth, indicating significant sediment transport. Extrapolating this data to the entire upper portion of the yardang field (25 km²) suggests a total gravel movement ranging from 2617.3 m³ to 7852.7 m³ over the 5-year period. This would be about 523.5 m³ to 1570.5 m^3 of gravel movement every year.

Analysis of gravel samples (FIGURE 25) showed that upwind samples were

Figure 25; This map shows the path traveled in red along with eleven sites where gravel pictures (blue) and samples (green) were collected.

larger (8-15 mm), more angular, and contained little to no quartz. Conversely, downwind samples were smaller (2.5-3 mm), very well-rounded, and contained up to 50% quartz (FIGURE 26).

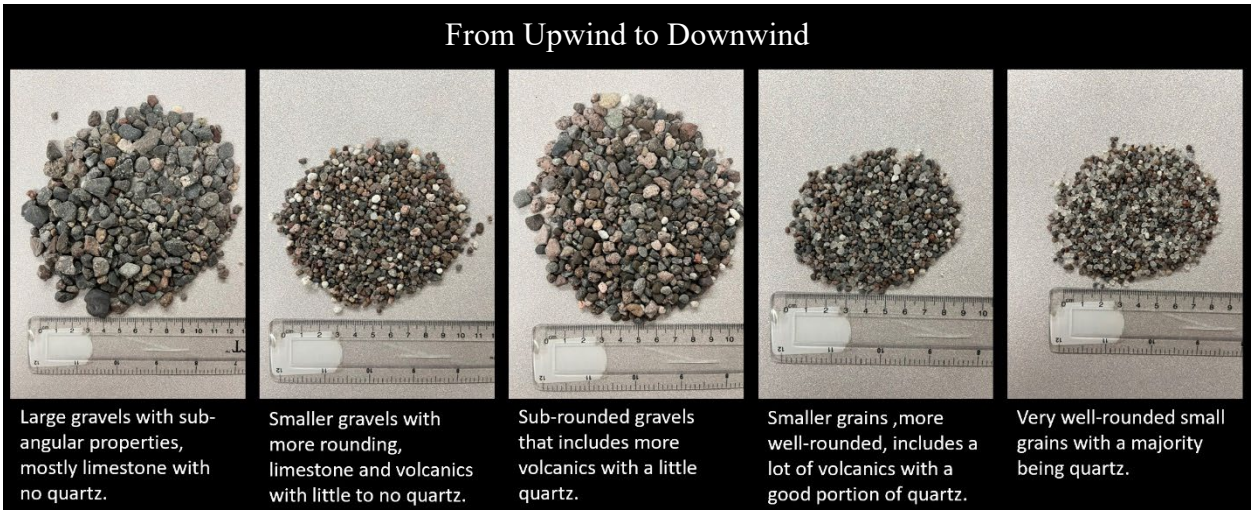

Figure 26; Gravel sample results from upwind to downwind with a description of size, shape, sorting and composition below the images.

The evidence supporting a staged progression model (FIGURE 27) is multifaceted. It includes the distinct differences in yardang and gravel abundances

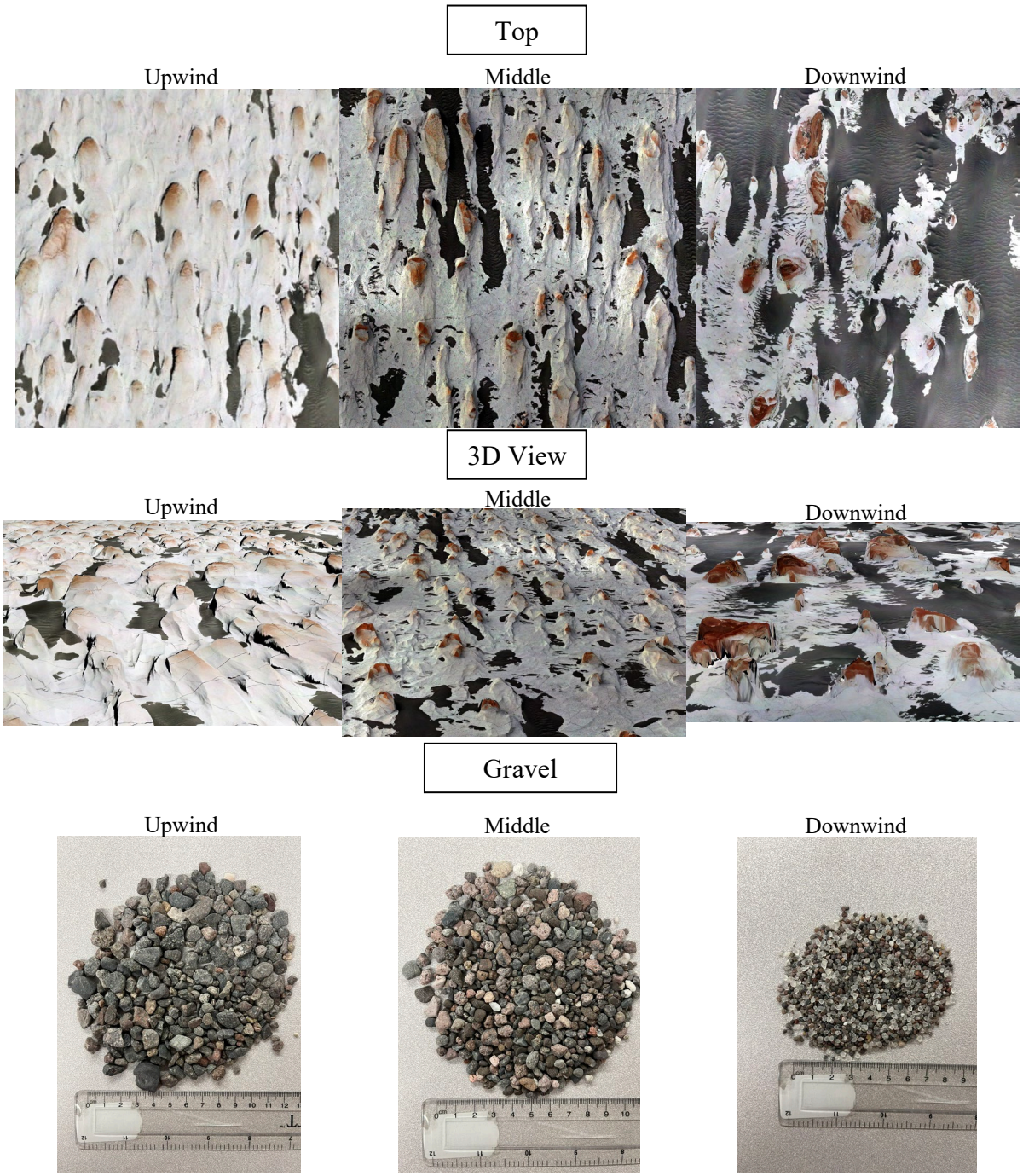

Figure 27; Three pictures showing an upper, middle and lower portion of the Campo de Piedra Pomez yardangs from and overhead and oblique view and gravel samples from each portion. Going from upwind to downwind a pattern can be observed of smaller to larger yardangs and gravels go from larger, more angular and no quartz to smaller, more rounded and lots of quartz. This shows that the gravel must blow through the field and aid in the formation and erosion of the yardangs.

observed upwind versus downwind, as well as the variations in gravel size, shape, and composition. Upwind, the larger, less rounded gravel with minimal quartz suggests minimal transport and erosion, consistent with the presence of less mature yardangs. Conversely, downwind, the smaller, well-rounded, quartz-rich gravel points to prolonged transport and erosional processes, which aligns with the more mature yardangs found in these areas. These observations collectively support the notion that yardangs evolve through a series of stages influenced by their position relative to prevailing winds.

Another piece of evidence for this staged progression model is the slope-removed DEMs (FIGURE 21) collected during the 2019 and 2024 field excursions. They indicate that the average height of yardangs upwind is about 7.3-9.5 m, whereas the average height downwind is 11.6-12.3 m. The observed increase in yardang height downwind is a critical aspect of this model, as it suggests that the more mature yardangs have been exposed to longer periods of wind erosion, leading to their taller, more developed structures. This increase in height, coupled with the progressive rounding and reduction in gravel size, provides strong support for the staged progression model, demonstrating the dynamic interplay between erosional forces and landscape evolution.

In an attempt to further support this model, the number of yardangs larger than 5 m^2 in each orthomosaic was calculated to identify a pattern that might distinguish incipient from mature yardangs along the upwind-to-downwind continuum. However, the results revealed a random distribution of yardangs in each region, with no discernible pattern.

Analysis of Digital Elevation Models (DEMs) revealed a significant correlation between higher elevations and a greater concentration of yardangs (FIGURE 28). These elevated areas, consistently identified across multiple images, may act as 'seed regions' for yardang formation, serving as the initial points where the staged progression model begins. Seed regions are localized areas where initial conditions—such as increased wind exposure, more resistant bedrock, and concentrated erosive forces—are optimal for the early stages of yardang development. In these regions, the interaction of elevation with prevailing wind dynamics creates micro-environments that foster the early stages of yardangs, as described in the staged progression model. Over

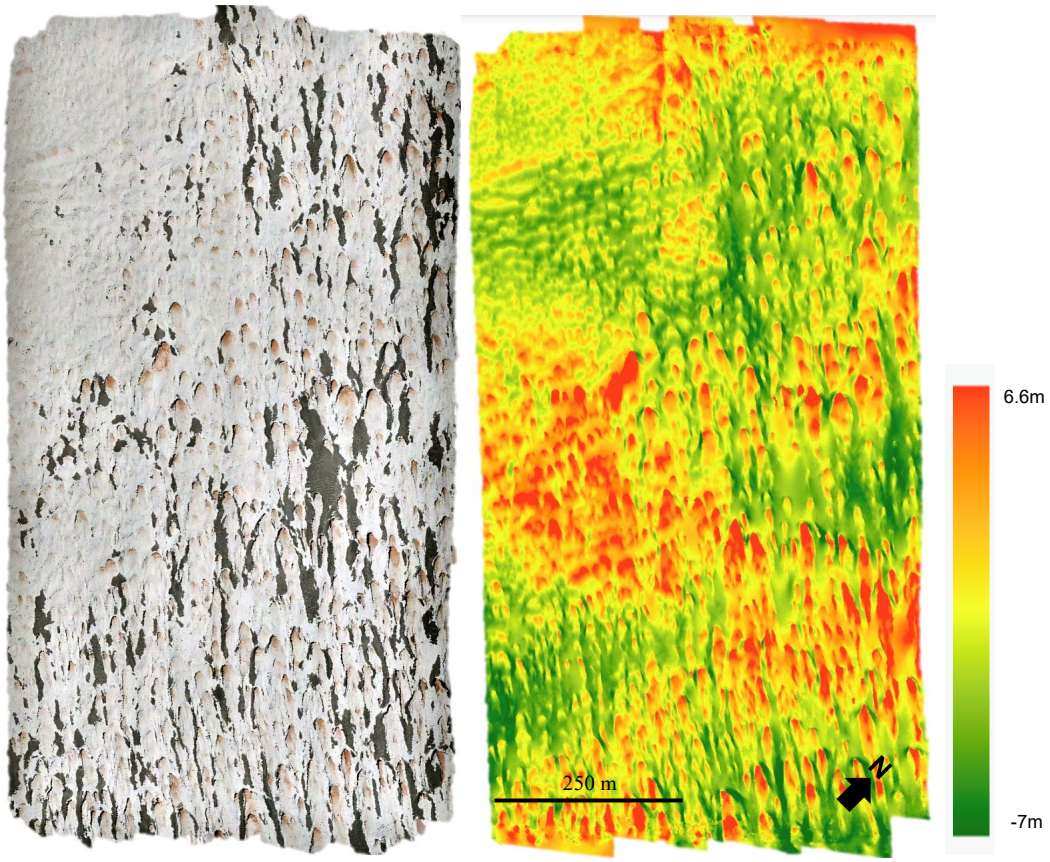

Figure 28; Orthomosaic (left) and a Digital Elevation Model (right) showing that a higher proportion of yardangs are located on slightly elevated platforms.

time, as these seed regions are subjected to ongoing wind erosion, they evolve into more mature yardangs, progressing through the stages outlined in the model. Thus, the concept of seed regions not only explains the initial formation of yardangs but also integrates seamlessly into the broader framework of the staged progression model, providing a comprehensive understanding of how localized factors drive the evolution of these landforms within the studied area.

These results provide a view into the dynamic interactions between geological features and aeolian processes, offering clear support for the staged progression model of yardang evolution in the CPP. By revealing how localized factors, such as seed regions and wind dynamics, drive the formation and maturation of yardangs, this study lays a foundation for further exploratory and comparative research.

7 Discussion

The influence of prevailing winds on Puna landscape morphology is demonstrated by the observed trends in yardang distribution and gravel movement. The distribution of yardangs is intricately linked to their exposure to dominant wind patterns; yardangs in the northwest appear younger and less developed, while those in the southeast exhibit signs of greater maturity, indicating a prolonged exposure to erosional processes. This analysis aligns with the staged progression model of yardang formation, which posits that yardangs evolve from smaller, incipient forms into larger, more mature structures as they are exposed to sustained wind erosion. This observation is consistent with findings from Favaro et al. (2021) in the CPP region and with similar studies in the Lut and Kumtagh Deserts by Ghodsi (2017) and Dong et al. (2011).

The staged progression model is further supported by the differences in yardang maturity across the field, where yardangs in the northwest, exposed to primary wind influx, may be younger and incipient, while those towards the southeast appear more mature. This could be due to differences in the ignimbrite properties upwind vs downwind. However, McDougall's (2022) research shows that the field of ignimbrite is relatively uniform.

The comparison of high-resolution drone imagery with lower-resolution satellite imagery highlighted significant differences in identifying and classifying smaller yardangs and finer morphological details. This significant discrepancy in resolution raises concerns that satellite imagery of Martian landforms, such as the Medusae Fossae Formation, may overlook or inaccurately classify smaller, yet critical, geomorphological features. Using high-resolution imagery in the Puna provides valuable analogs for planetary exploration and helps develop methods to infer the presence of smaller details on Mars and other extraterrestrial bodies, where surface features may be underrepresented due to resolution limitations.

Significant variations in gravel size, shape, and composition from upwind to downwind areas underscore the influence of aeolian processes on sediment transport across the yardang field. The transition from larger, angular gravel upwind to smaller, well-rounded, quartz-rich gravel downwind suggests that strong, consistent winds play a

critical role in gravel transport and maturation. These observations provide insights into sediment transport dynamics in arid environments but also support the staged progression model by illustrating how gravel characteristics evolve alongside yardangs as they progress through different stages of development.

Observations indicate that the quartz originates from within the volcanic ash flow tuff that the yardangs are sculpted in. As the yardangs erode due to the wind-blown gravel, the quartz persists due to its hardness. However, it is important to note that the quartz is very well rounded. The rounded nature of the quartz could result from several processes: it might have been rounded during the volcanic eruption, sourced from outside the yardang field, or gradually worn down by wind-driven erosion as it migrates across the landscape.

The change detection analysis over the five-year period showed stability in yardang structures but variations in gravel distribution, highlighting the ongoing influence of wind dynamics on sediment transport and deposition. The near equivalence in the areas of gravel presence and absence suggests a dynamic balance where wind continuously redistributes gravel, emphasizing the significant role of wind in gravel transport and the dynamic nature of sediment redistribution within the yardang field.

By integrating of these findings into the staged progression model, this research enhances our understanding of yardang evolution in the Puna and provides valuable insights that can be applied to similar aeolian landscapes on Earth and other planetary bodies. This study, therefore, lays the groundwork for future research into the processes that shape arid landscapes, offering a comprehensive framework for exploring the complexities of yardang formation and evolution in diverse environments.

8 Conclusion

This investigation into the meso-yardangs of the Campo de Piedra Pomez (CPP) region within the Puna-Altiplano Plateau has provided insights into the interaction between geological evolution and aeolian processes that shape the landscape. These findings contribute to the broader understanding of yardangs worldwide.

Employing high-resolution drone and satellite imagery, along with photogrammetry and Digital Elevation Models (DEMs), this study successfully classified

three different landforms using the high-resolution drone imagery and examined them across the field. This led to the discovery of a clear gradient in yardang distribution from windward to leeward, illustrating significant variations in gravel coverage and bedrock exposure. The detailed methodologies employed underscore the critical role of advanced technologies in enhancing the precision and depth of geomorphological studies.

Central to this study is the introduction of a nuanced staged progression model for yardang formation, which posits that yardangs exhibit increasing maturity from upwind to downwind. This model not only explains the observed spatial dynamics of erosional processes but also provides a framework for predicting the evolution of yardang fields over time. By linking yardang maturity with their position relative to prevailing winds, the staged progression model underscores the importance of spatial context in understanding the intricate relationship between wind dynamics and landscape evolution.

Ongoing and future research in the CPP region, bolstered by remote sensing technologies, promise to deepen insights into the geomorphological processes shaping these landscapes. Beyond terrestrial implications, this study offers valuable parallels for understanding similar landforms on extraterrestrial bodies such as Mars, Venus, and Titan. This research advances knowledge of aeolian processes both on Earth and in planetary environments, paving the way for future exploration and discovery in planetary geology and geomorphology.

References

Báez, Walter, et al. “Pulsating Flow Dynamics of Sustained, Forced Pyroclastic Density Currents: Insights from a Facies Analysis of the Campo de La Piedra Pómez Ignimbrite, Southern Puna, Argentina.” *Bulletin of Volcanology*, vol. 82, no. 7, 2020, p. 53, https://doi.org/10.1007/s00445-020-01385-5.

Barchyn, Thomas E., and Chris H. Hugenholtz. “Yardang Evolution from Maturity to Demise.” *Geophysical Research Letters*, vol. 42, no. 14, July 2015, pp. 5865–71, https://doi.org/10.1002/2015GL064477.

Barnes, Jason W., et al. “Production and Global Transport of Titan’s Sand Particles.” *Planetary Science*, vol. 4, no. 1, 2015, p. 1, https://doi.org/10.1186/s13535-015-0004-y.

Carrapa, B., and P. G. DeCelles. “Eocene Exhumation and Basin Development in the Puna of Northwestern Argentina: EOCENE BASIN DEVELOPMENT IN NW ARGENTINA.” *Tectonics*, vol. 27, no. 1, 2008, p. n/a-n/a, https://doi.org/10.1029/2007TC002127.

Chahid, Driss, et al. “First Identification of Yardangs in the Dakhla Region (Southern Morocco).” *Bulletin de l’Institut Scientifique Rabat Section Sciences de La Terre*, no. 45, 2023, p. 15, https://shs.hal.science/halshs-04069885.

Coutand, Isabelle, et al. “Style and History of Andean Deformation, Puna Plateau, Northwestern Argentina.” *Tectonics*, vol. 20, no. 2, 2001, pp. 210–34, https://doi.org/10.1029/2000TC900031.

De Silva, S. L., et al. “Gravel-Mantled Megaripples of the Argentinean Puna: A Model for Their Origin and Growth with Implications for Mars.” *Geological Society of America Bulletin*, vol. 125, no. 11–12, Nov. 2013, pp. 1912–29, https://doi.org/10.1130/B30916.1.

De Silva, S.L., J. Roberge, et al. “Magmatic Evolution and Architecture of an Arc-Related, Rhyolitic Caldera Complex: The Late Pleistocene to Holocene Cerro Blanco Volcanic Complex,

Southern Puna, Argentina." *Geosphere*, vol. 18, no. 2, Apr. 2022, pp. 394–423, https://doi.org/10.1130/GES02294.1.

De Silva, S.L., J. E. Bailey, et al. "Yardangs in Terrestrial Ignimbrites: Synergistic Remote and Field Observations on Earth with Applications to Mars." *Planetary and Space Science*, vol. 58, no. 4, 2010, pp. 459–71, https://doi.org/10.1016/j.pss.2009.10.002.

Ding, Zhaojing, et al. "Yardangs on Earth and Implications to Mars: A Review." *Geomorphology*, vol. 364, 2020, p. 107230, https://doi.org/10.1016/j.geomorph.2020.107230.

Dong, Zhibao, et al. "Geomorphology and Origin of Yardangs in the Kumtagh Desert, Northwest China." *Geomorphology*, vol. 139–140, 2012, pp. 145–54, https://doi.org/10.1016/j.geomorph.2011.10.012.

Dromart, G., et al. "Deposition and Erosion of a Light-Toned Yardang-Forming Unit of Mt Sharp, Gale Crater, Mars." *Earth and Planetary Science Letters*, vol. 554, 2021, p. 116681, https://doi.org/10.1016/j.epsl.2020.116681.

Ehsani, Amir Houshang, and Friedrich Quiel. "Application of Self Organizing Map and SRTM Data to Characterize Yardangs in the Lut Desert, Iran." *Remote Sensing of Environment*, vol. 112, no. 7, 2008, pp. 3284–94, https://doi.org/10.1016/j.rse.2008.04.007.

Favaro, Elena A., et al. "Antecedent Controls on the Spatial Organization of Yardangs on the Puna Plateau, North-western Argentina." *Earth Surface Processes and Landforms*, vol. 46, no. 15, 2021, pp. 3063–77, https://doi.org/10.1002/esp.5212.

Fernández, Osvaldo A., and C. A. Busso. "Arid and Semiarid Rangelands of Argentina." *Climate Variability Impacts on Land Use and Livelihoods in Drylands*, edited by Mahesh K. Gaur and Victor R. Squires, Springer International Publishing, 2018, pp. 261–91, https://doi.org/10.1007/978-3-319-56681-8_13.

Ganey, Terra M., et al. “Reassessment of the Volumes of Sediment Sources and Sinks on Venus.” *The Planetary Science Journal*, vol. 4, no. 1, Jan. 2023, p. 9, https://doi.org/10.3847/PSJ/aca521.

Ghodsi, M. “Morphometric Characteristics of Yardangs in the Lut Desert, Iran: Desert (2008-0875).” *Desert (2008-0875)*, vol. 22, no. 1, Winter/Spring ///Winter/Spring2017 2017, pp. 21–29, https://search.ebscohost.com/login.aspx?direct=true&db=aph&AN=124218644&site=ehost-live.

Goldsmith, Yonaton, et al. “From Dust to Varnish: Geochemical Constraints on Rock Varnish Formation in the Negev Desert, Israel.” *Geochimica et Cosmochimica Acta*, vol. 126, 2014, pp. 97–111, https://doi.org/10.1016/j.gca.2013.10.040.

Goudie, Andrew S. “Mega-Yardangs: A Global Analysis.” *Geography Compass*, vol. 1, no. 1, 2007, pp. 65–81, https://doi.org/10.1111/j.1749-8198.2006.00003.x.

Greeley, Ronald, Andrew Skypeck, et al. “Martian Aeolian Features and Deposits: Comparisons with General Circulation Model Results.” *Journal of Geophysical Research: Planets*, vol. 98, no. E2, Feb. 1993, pp. 3183–96, https://doi.org/10.1029/92JE02580.

Greeley, Ronald, Kelly Bender, et al. “Wind-Related Features and Processes on Venus: Summary of Magellan Results.” *Icarus*, vol. 115, no. 2, 1995, pp. 399–420, https://doi.org/10.1006/icar.1995.1107.

Hu, Chengqing, et al. “Yardang Geometries in the Qaidam Basin and Their Controlling Factors.” *Geomorphology*, vol. 299, 2017, pp. 142–51, https://doi.org/10.1016/j.geomorph.2017.09.029.

Khawja, S., et al. “Tesserae on Venus May Preserve Evidence of Fluvial Erosion.” *Nature Communications*, vol. 11, no. 1, Nov. 2020, p. 5789, https://doi.org/10.1038/s41467-020-19336-1.

Kite, Edwin S., et al. “Stratigraphy of Aeolis Dorsa, Mars: Stratigraphic Context of the Great River Deposits.” *Icarus*, vol. 253, 2015, pp. 223–42, https://doi.org/10.1016/j.icarus.2015.03.007.

Liu, Jia, et al. “Mapping and Spatial Statistical Analysis of Mars Yardangs.” *Planetary and Space Science*, vol. 192, 2020, p. 105035, https://doi.org/10.1016/j.pss.2020.105035.

Lorenz, Ralph D., et al. “The Seas of Titan.” *Eos, Transactions American Geophysical Union*, vol. 84, no. 14, Apr. 2003, pp. 125–32, https://doi.org/10.1029/2003EO140002.

MacKenzie, Shannon M., et al. “Sediment-Moving Winds and Abrasion on Titan: Implications for Yardangs.” *Icarus*, vol. 394, 2023, p. 115433, https://doi.org/10.1016/j.icarus.2023.115433.

McDougall, Dylan S. “Yardang Morphometry and Substrate Properties in Ignimbrites of the Campo Piedra Pomez, Argentina Compared with the Medusae Fossae Formation, Mars.” Brigham Young University, United States -- Utah, 2022. *ProQuest*, https://byu.idm.oclc.org/login/?url=https://www.proquest.com/dissertations-theses/yardang-morphometry-substrate-properties/docview/2901811915/se-2.

Northrup, Dustin S. “A Geomorphological Study of Yardangs in China, the Altiplano/Puna of Argentina, and Iran as Analogs for Yardangs on Titan.” Brigham Young University, United States -- Utah, 2018. *ProQuest*, https://byu.idm.oclc.org/login/?url=https://www.proquest.com/dissertations-theses/geomorphological-study-yardangs-china-altiplano/docview/2442598537/se-2.Paillou, Philippe, et al. “Radar Scattering of Linear Dunes and Mega-Yardangs: Application to Titan.” *Icarus*, vol. 270, 2016, pp. 211–21, https://doi.org/10.1016/j.icarus.2015.07.038.

Pelletier, Jon D., et al. “Controls on Yardang Development and Morphology: 1. Field Observations and Measurements at Ocotillo Wells, California.” *Journal of Geophysical Research: Earth Surface*, vol. 123, no. 4, 2018, pp. 694–722, https://doi.org/10.1002/2017JF004461.

---. “Controls on Yardang Development and Morphology: 2. Numerical Modeling.” *Journal of Geophysical Research: Earth Surface*, vol. 123, no. 4, 2018, pp. 723–43, https://doi.org/10.1002/2017JF004462.

Radebaugh, J., et al. “Dunes on Titan Observed by Cassini Radar.” *Icarus*, vol. 194, no. 2, 2008, pp. 690–703, https://doi.org/10.1016/j.icarus.2007.10.015.

Sarmast, Masoomeh, et al. “Soil and Desert Varnish Development as Indicators of Landform Evolution in Central Iranian Deserts.” *CATENA*, vol. 149, 2017, pp. 98–109, https://doi.org/10.1016/j.catena.2016.09.003.

Turner, Darren, et al. “An Automated Technique for Generating Georectified Mosaics from Ultra-High Resolution Unmanned Aerial Vehicle (UAV) Imagery, Based on Structure from Motion (SfM) Point Clouds.” *Remote Sensing*, vol. 4, no. 5, May 2012, pp. 1392–410, https://doi.org/10.3390/rs4051392.

Villarreal, Carlos Alberto, et al. “Workflow for Capturing Information and Characterizing Difficult-to-Access Geological Outcrops Using Unmanned Aerial Vehicle-Based Digital Photogrammetric Data.” *Journal of Industrial Information Integration*, vol. 26, 2022, p. 100292, https://doi.org/10.1016/j.jii.2021.100292.

Ward, A. W., and Ronald Greeley. “Evolution of the Yardangs at Rogers Lake, California.” *Geological Society of America Bulletin*, vol. 95, no. 7, 1984, p. 829, https://doi.org/10.1130/0016-7606(1984)95<829:EOTYAR>2.0.CO;2.